อนุภาคระดับนาโนเมตรลูกผสมพอลิฟีนอล-ซิงก์ออกไซด์ตอบสนองต่อค่าพีเอชสำหรับการนำส่งยาต้านมะเร็ง

นายปวัศนัย สมุทรประเสริฐ

จุฬาลงกรณ์มหาวิทยาลัย
Chulalongkorn University

บทคัดย่อและแฟ้มข้อมูลฉบับเต็มของวิทยานิพนธ์ตั้งแต่ปีการศึกษา 2554 ที่ให้บริการในคลังปัญญาจุฬาฯ (CUIR)
เป็นแฟ้มข้อมูลของนิสิตเจ้าของวิทยานิพนธ์ ที่ส่งผ่านทางบัณฑิตวิทยาลัย
The abstract and full text of theses from the academic year 2011 in Chulalongkorn University Intellectual Repository (CUIR)
are the thesis authors' files submitted through the University Graduate School.

วิทยานิพนธ์นี้เป็นส่วนหนึ่งของการศึกษาตามหลักสูตรปริญญาวิทยาศาสตรมหาบัณฑิต
สาขาวิชาเคมี ภาควิชาเคมี
คณะวิทยาศาสตร์ จุฬาลงกรณ์มหาวิทยาลัย
ปีการศึกษา 2558
ลิขสิทธิ์ของจุฬาลงกรณ์มหาวิทยาลัย

pH-RESPONSIVE POLYPHENOL-ZINC OXIDE HYBRID NANOPARTICLES FOR ANTICANCER DRUG DELIVERY

Mr. Pawatsanai Samutprasert

A Thesis Submitted in Partial Fulfillment of the Requirements
for the Degree of Master of Science Program in Chemistry
Department of Chemistry
Faculty of Science
Chulalongkorn University
Academic Year 2015

Copyright of Chulalongkorn University

Thesis Title	pH-RESPONSIVE POLYPHENOL-ZINC OXIDE HYBRID NANOPARTICLES FOR ANTICANCER DRUG DELIVERY
By	Mr. Pawatsanai Samutprasert
Field of Study	Chemistry
Thesis Advisor	Associate Professor Supason Wanichwecharungruang, Ph.D.

Accepted by the Faculty of Science, Chulalongkorn University in Partial Fulfillment of the Requirements for the Master's Degree

.....Dean of the Faculty of Science
(Associate Professor Polkit Sangvanich, Ph.D.)

THESIS COMMITTEE

.....Chairman
(Associate Professor Vudhichai Parasuk, Ph.D.)

.....Thesis Advisor
(Associate Professor Supason Wanichwecharungruang, Ph.D.)

.....Examiner
(Assistant Professor Pattara Thiraphibundet, Ph.D.)

.....Examiner
(Numpon Insin, Ph.D.)

.....External Examiner
(Kriengsak Lirdprapamongkol, Ph.D.)

ปวัศนัย สมุทรประเสริฐ : อนุภาคระดับนาโนเมตรลูกผสมพอลิฟีนอล-ซิงก์ออกไซด์ตอบสนองต่อค่าพีเอชสำหรับการนำส่งยาต้านมะเร็ง (pH-RESPONSIVE POLYPHENOL-ZINC OXIDE HYBRID NANOPARTICLES FOR ANTICANCER DRUG DELIVERY) อ.ที่ปรึกษาวิทยานิพนธ์หลัก: รศ. ดร.ศุภศร วนิชเวชารุ่งเรือง, 66 หน้า.

วัสดุระดับนาโนเมตรลูกผสมอินทรีย์อนินทรีย์เป็นวัสดุที่สร้างมาจากการเกิดอันตรกิริยากันระหว่างสารอินทรีย์กับอนินทรีย์ โดยจะได้วัสดุลูกผสมที่มีคุณสมบัติที่ดีขึ้นในการประยุกต์ใช้ในงานต่างๆ โดยทั่วไปอนุภาคระดับนาโนเมตรซิงก์ออกไซด์แสดงฤทธิ์ทางด้านชีวภาพเช่นการต้านมะเร็งและการต้านแบคทีเรีย รวมทั้งมีงานจำนวนมากที่รายงานประสิทธิภาพที่ดีของการต้านมะเร็งของสารสกัดพอลิฟีนอลจากชา ดังนั้นสำหรับงานวิจัยนั้นสนใจในการสังเคราะห์วัสดุระดับนาโนเมตรลูกผสมอินทรีย์อนินทรีย์จากสารสกัดพอลิฟีนอลจากชาซิงก์ออกไซด์สำหรับการประยุดต์ในการนำส่งยามะเร็งดอกโซรูบิซิน และแพคลิแท็กเซล รวมทั้งทำการพิสูจน์กลไกการเข้าเซลล์ผ่านวิถีเอนโดไซโตซิสและกลไกการปลดปล่อยสารของอนุภาคที่สังเคราะห์ขึ้น

จุฬาลงกรณ์มหาวิทยาลัย
Chulalongkorn University

ภาควิชา เคมี ลายมือชื่อนิสิต .....

สาขาวิชา เคมี ลายมือชื่อ อ.ที่ปรึกษาหลัก .....

ปีการศึกษา 2558

5672015223 : MAJOR CHEMISTRY

KEYWORDS: HYBRID NANOMATERIALS / ORGANIC-INORGANIC / ZINC OXIDE / TEA POLYPHENOL / DRUG DELIVERY

PAWATSANAI SAMUTPRASERT: pH-RESPONSIVE POLYPHENOL-ZINC OXIDE HYBRID NANOPARTICLES FOR ANTICANCER DRUG DELIVERY. ADVISOR: ASSOC. PROF. SUPASON WANICHWECHARUNGRUANG, Ph.D., 66 pp.

Organic-inorganic hybrid nanomaterial fabricated by the interactions between organic and inorganic matters has attracted great deal of attention for the introduction of novel functions. Zinc oxide nanoparticles show many biological activities such as anticancer and antibacterial. The tea polyphenol has many reported as the potential anticancer agent. In this work, we interested in combination of tea polyphenol and zinc oxide as the organic-inorganic hybrid nanomaterial for delivery antitumor agents. Herein, we have developed drug delivery system from the complexation of zinc oxide and natural product extract. We showed the particles fabrication, characterization and drug delivery application of this organic-inorganic hybrid material. Delivering of drugs (doxorubicin and paclitaxel) by the tea polyphenol-ZnO nanoparticles into cancerous cells was achieved. We also verified that the particles can be taken up into the cancer cell by endocytosis mechanism and endosome burst to release chemicals to cytosol as the mechanism of releasing of the particles.

จุฬาลงกรณ์มหาวิทยาลัย
Chulalongkorn University

Department: Chemistry Student's Signature .....

Field of Study: Chemistry Advisor's Signature .....

Academic Year: 2015

ACKNOWLEDGEMENTS

First of all, I would like to express my sincere appreciation to my thesis advisor, Associate Professor Dr. Supason Wanichwecharungruang for her helpful supervision, invaluable assistance and generous encouragement to fulfill my achievement.

I would like to thank all members of the committee Associate Professor Dr. Vudhichai Parasuk, Assistant Professor Dr. Pattara Thiraphibundet and Dr.Numpon Insin their time and recommendations as the committee members.

I gratefully appreciate to Miss Khajeelak Chiableam, Dr.Kiengsak Lirdprapamongkol from Chulabhorn Research Institute for theirs advises, guidance and helps in cytotoxicity test.

I would not forget to thank Center of Excellence on Petrochemical and Materials Technology, the 90th anniversary of Chulalongkorn University fund (Ratchadaphiseksomphot Endowment Fund) at Chulalongkorn University and the Graduate School, Chulalongkorn University for scholarship and financial support.

Last but not least, I would like to specially thank my family, my friends and research groups for their advice and encouragement throughout my master study.

CONTENTS

Page

THAI ABSTRACT iv

ENGLISH ABSTRACT v

ACKNOWLEDGEMENTS vi

CONTENTS vii

LIST OF TABLES xi

LIST OF FIGURES xii

LIST OF SCHEMES xvi

LIST OF ABBREVIATIONS xvii

CHAPTER I INTRODUCTION 1

1.1 Hybrid nanomaterial 1

1.2 Literature review of hybrid nanomaterial for drug delivery 2

1.3. The global statistic of cancer disease 3

1.4 Literature of application drug delivery system of cancer drugs 4

1.5. Endocytosis pathway 5

1.5. Endocytosis pathway 5

1.6 Zinc oxide nanoparticles 6

1.6.1 Crystal Structure of Zinc Oxide 6

1.6.2. Type of zinc oxide synthesis 8

1.6.3 Hydro/Solvothermal synthesis 8

1.6.4. Solubility of zinc oxide in acid solution 8

1.7. Application of zinc oxide in drug delivery. 9

1.8. Anti-tumor activity of Zn ions in cancer cells 9

จุฬาลงกรณ์มหาวิทยาลัย
CHULALONGKORN UNIVERSITY

Page

1.9 Synergistic effect between zinc and tea polyphenol.....10

1.10 Objective and scope of work.....11

CHAPTER II EXPERIMENTAL.....12

2.1 Materials and Chemicals.....12

2.1.1 Media culture and chemical reagent for cell culture and treatment.13

2.2 Preparation of tea polyphenol extract.....13

2.2.1 Quantification of each component in tea polyphenol extract by HPLC (High Performance Liquid Chromatography).....13

2.2.2. Calibration curve.....14

2.3 Synthesis of tea polyphenol-zinc oxide nanoparticles (TP-ZnO).....14

2.3.1 Optimization on the amount of tea polyphenol used.....14

2.4 Synthesis of Curcumin-zinc oxide nanoparticles (CM-ZnO) and α-mangostin -zinc oxide nanoparticles (MG-ZnO).....15

2.5 Loading of drugs on TP-ZnO nanoparticles.....15

2.6 In Vitro antitumor assay.....16

2.6.1 Cell culture.....16

2.6.2 Cell viability assay.....16

2.7 Cellular uptake of loaded DOX-TP-ZnO.....17

CHAPTER III RESULTS AND DISCUSSION.....18

3.1 Quantification of each component in tea polyphenol extract by HPLC (High Performance Liquid Chromatography).....18

3.2 Synthesis of tea polyphenol-zinc oxide nanoparticles (TP-ZnO).....20

3.2.1 Optimization on the amount of tea polyphenol extract used.....20

จุฬาลงกรณ์มหาวิทยาลัย
Chulalongkorn University

Page

3.3 Synthesis of Curcumin-zinc oxide nanoparticles (CM-ZnO) and α-mangostin -zinc oxide nanoparticles (MG-ZnO).....23

3.4 Morphology of all products 24

3.5 Crystal structure analysis 27

3.6 Chemicals interaction of organic matters with zinc oxide in the nanoparticles 28

3.7 The organic matters inside zinc oxide nanoparticles 32

3.8 Interactions between the natural compounds (tea polyphenol, curcumin and α-mangostin) and the ZnO crystals within the hybrid nanoparticles. ..35

3.9 Functional group on surface of all particles (TP-ZnO, CM-ZnO and MG-ZnO nanoparticles) 39

3.10 Loading of drugs on TP-ZnO nanoparticles 41

3.11 Interaction of the cancer drug with TP-ZnO nanoparticles.....42

3.12 pH responsive dissolution test using turbidity measurement 44

3.13 Cytotoxicity test with cancer cells 47

3.13.1 Cytotoxicity test of ZnO, TP-ZnO, EGCG-ZnO nanoparticles, tea polyphenol extract and epigallocatechin-3-gallate free compound. .47

3.13.2 Cytotoxicity test of paclitaxel loaded TP-ZnO (TP-ZnO-TX) and doxorubicin TP-ZnO (TP-ZnO-DOX). 48

3.14 Cellular uptake of loaded DOX-TP-ZnO 51

CHAPTER IV CONCLUSION 55

APPENDIX 56

APPENDIX A 57

Calculation of %encapsulation efficiency and loading content of drug loaded on the particles 57

Chulalongkorn University

Page

APPENDIX B 61

REFERENCES 62

VITA.....66

จุฬาลงกรณ์มหาวิทยาลัย
Chulalongkorn University

LIST OF TABLES

Table Page

1.1 Physical properties of ZnO 7

2.1 Weight ratio between tea polyphenol and zinc chloride. 15

3.1 Contents of the four major components in crude methanol extract. 19

3.2 SEM results of prepared tea polyphenol-zinc oxide nanoparticles (TP-ZnO) 21

3.3 The amount of organic matter in each nanoparticles 26

3.4 Encapsulation efficiency and loading capacity of doxorubicin and paclitaxel on the TP-ZnO nanoparticles..... 41

จุฬาลงกรณ์มหาวิทยาลัย
Chulalongkorn University

LIST OF FIGURES

Figure Page

Figure 1.1 Interactions of organic applied in hybrid materials. 1

Figure 1.2 The distribution of common cancer around the world in male 3

Figure 1.3 Crystal structure of zinc oxide 6

Figure 1.4 The equation display the zinc oxide formation. 8

Figure 1.5 The equation display the zinc oxide react with acid. 8

Figure 3.1 Chromatogram of tea polyphenol extract (TP). 18

Figure 3.2 SEM results of (A) α-Mangostin-zinc oxide (MG-ZnO), (B) Curcumin-zinc oxide (CM-ZnO) and (C) Tea polyphenol zinc oxide (TP-ZnO) nanoparticles..... 25

Figure 3.3 TEM micrographs of (A) Mangostin-zinc oxide (MG-ZnO), (B) Curcumin-zinc oxide (CM-ZnO) and (C) Tea polyphenol zinc oxide (TP-ZnO) nanoparticles..... 25

Figure 3.4 The dimension and of each product (A) Mangostin-zinc oxide (MG-ZnO), (B) Curcumin-zinc oxide (CM-ZnO) and (C) Tea polyphenol zinc oxide (TP-ZnO) nanoparticles. 25

Figure 3.5 X-ray diffraction patterns of TP-ZnO (red line), MG-ZnO (blue line), CM-ZnO (green line) and standard ZnO crystal (black line). 27

Figure 3.6 FT-IR spectra of TP-ZnO nanoparticles (red line), tea polyphenol extract (blue line) and zinc oxide crystal standard (purple line). 30

Figure 3.7 FT-IR spectra of MG-ZnO nanoparticles (red line), α-mangostin (light blue line) and zinc oxide crystal standard (purple line). 30

Figure 3.8 FT-IR spectra of CM-ZnO nanoparticles (red line), curcumin (green line) and zinc oxide crystal standard (purple line). 31

Figure 3.9 FT-IR spectra of composite of curcumin/ZnO (CM/ZnO,blue line), α-mangostin/ZnO(MG/ZnO, red line) and teapolyphenol/ZnO(TP/ZnO, green line) nanoparticles 31

Figure 3.10 UV absorption spectra of free tea polyphenol (TP, orange line) and TP from TP-ZnO (blue line). 33

Figure 3.11 UV absorption spectra of free curcumin (CM, yellow line) and CM from CM-ZnO (green line). 33

Figure 3.12 UV absorption spectra of free α-mangostin (MG, red line) and MG from MG-ZnO (purple line). 34

Figure 3.13 Thermo gravimetric curves (TG) and Differential themo gravimetric (DTG) curves of free tea polyphenol (red line), TP-ZnO (purple line) and standard zinc oxide (pale blue line). 35

Figure 3.14 Thermo gravimetric curves (TG) and Differential themo gravimetric (DTG) curves of free curcumin (yellow line) and CM-ZnO (red line). 36

Figure 3.15 Thermo gravimetric curves (TG) and Differential thermo gravimetric (DTG) curves of free α-mangostin (purple line), MG-ZnO (green line) and standard zinc oxide (pale blue line) 36

Figure 3.16 Differential scanning calorimetric thermaograms of tea polyphenol(blue line), TP-ZnO (red line) and standard ZnO (green line) 37

Figure 3.17 Differential scanning calorimetric thermaograms of curcumin(pink line) and CM-ZnO (blue line) 37

Figure 3.18 Differential scanning calorimetric thermaograms of α-mangostin(pink line) and MG-ZnO (brown line). 38

Figure 3.19 Differential scanning calorimetric thermaograms of Standard ZnO (green line) 38

Figure3.20 XPS spectra of TP-ZnO nanoparticles (row A), CM-ZnO nanoparticles (row B) and MG-ZnO nanoparticles (row C) 40

Figure 3.21 FT-IR spectra of doxorubicin (purple line), doxorubicin-loaded TP-ZnO nanoparticles (6.97±0.13 %w/w loading content, red line) and TP-ZnO nanoparticles (pink line). 43

Figure 3.22 FT-IR spectra of paclitaxel (purple line), paclitaxel-loaded TP-ZnO nanoparticles (6.67±0.15%w/w loading content, red line) and unloaded TP-ZnO nanoparticles (blue line). 43

Figure 3.23 Physical appearance of particles at pH=7 (left side) and pH=4.5 (right side). 45

Figure 3.24 Light transmission through ZnO(blue line), TP-ZnO(purple line), EGCG-ZnO(yellow line), CM-ZnO(red line) and MG-ZnO(green line) suspensions. 45

Figure 3.25 Light transmission through EGCG-ZnO(yellow line), TP-ZnO(purple line), TP-ZnO-DOX (gray line) and EGCG-ZnO-DOX(blue line) 46

Figure 3.26 Light transmission through EGCG-ZnO(yellow line), TP-ZnO(purple line), TP-ZnO-TX (red line) and EGCG-ZnO-TX(green line) 46

Figure 3.27 Cell viability of PC-3 cancer cell with zinc oxide crystal standard (ZnO, blue column), paclitaxel (TX, red column), tea polyphenol extract (TP, green column), TP-ZnO nanoparticles (purple column) and paclitaxel loaded TP-ZnO (TP-ZnO-TX, light blue column). 49

Figure 3.28 Cell viability of PC-3 cancer cell with zinc oxide crystal standard (ZnO, blue column), doxorubicin (DOX, red column), tea polyphenol extract (TP, green column), TP-ZnO nanoparticles (purple column) and doxorubicin loaded TP-ZnO (TP-ZnO-DOX, light blue column). 49

Figure 3.29 Cell viability of PC-3 cancer cell with zinc oxide crystal standard (ZnO, blue column), paclitaxel (TX, red column), epigallocatechin-3-gallate (EGCG, green column), EGCG-ZnO nanoparticles (purple column) and paclitaxel loaded EGCG-ZnO nanoparticles (TP-ZnO-TX, light blue column). 50

Figure 3.30 Cell viability of PC-3 cancer cell with zinc oxide crystal standard (ZnO, blue column), doxorubicin (DOX, red column), epigallocatechin-3-gallate (EGCG,

green column), EGCG-ZnO nanoparticles (purple column) and doxorubicin loaded EGCG-ZnO nanoparticles (EGCG-ZnO-TX, light blue column). 50

Figure 3.31 The complexation of zinc ions with zinquin ethyl ester 51

Figure 3.32 The confocal fluorescent picture: Zn^{2+} ions probs (First column), Early endosome (Second column), lysosome (Third column), Bright Field (Fourth column) and Merge (Fifth column) 53

Figure 3.33 The confocal fluorescent focus single cell images: Zn^{2+} ions prob (First column), early endosome (second column) and lysosome (third column). 54

Figure 4.1 The dimension and of each product (A) Mangostin-zinc oxide (MG-ZnO), (B) Curcumin-zinc oxide (CM-ZnO) and (C) Tea polyphenol zinc oxide (TP-ZnO) 55

Figure A-1 Calibration curve of doxorubicin at 230.nm 57

Figure A-2 Calibration curve of paclitaxel at 220.nm 59

จุฬาลงกรณ์มหาวิทยาลัย
Chulalongkorn University

LIST OF SCHEMES

Scheme Page

3.1 Synthesis of TP-ZnO nanoparticles through hydrothermal synthesis by nucleation of zinc oxide nucleus..... 20

3.2 Synthesis of CM-ZnO and MG-ZnO nanoparticles through hydrothermal synthesis by the nucleation of zinc oxide nucleus..... 23

จุฬาลงกรณ์มหาวิทยาลัย
Chulalongkorn University

LIST OF ABBREVIATIONS

TP	Tea polyphenol extract
CM	Curcumin
MG	α-mangostin
ZnO	Zinc oxide
%	Percent
ml	Militer
µg	Microgram
ppm	Part per million
min	Minute
h	Hour
g	Gram
w/w	Weight by weight
XPS	X-ray photoelectron spectroscopy
SEM	Scanning electron microscopy
TEM	Transmission electron microscopy
TGA	Thermo gravimetric analysis
HPLC	High performance liquid chromatography
XRD	X-ray diffraction
CLSM	Confocal laser scanning microscopy
UV-Visible	Ultraviolet/Visible
TEA	Triethlylamine
NaOH	Sodium hydroxide

จุฬาลงกรณ์มหาวิทยาลัย
CHULALONGKORN UNIVERSITY

$ZnCl_2$	Zinc chloride
MTT	3-(4,5-dimethylthiazol-2-yl)-2,5-diphenyltetrazolium bromide
ATCC	American Type Culture Collection
F-12k	Kaighn's Modification of Ham's F-12 Medium
%EE	Encapsulation efficiency
%loading	Loading capability

จุฬาลงกรณ์มหาวิทยาลัย
Chulalongkorn University

CHAPTER I

INTRODUCTION

1.1 Hybrid nanomaterial

Hybrid materials represent one of the most fabulous developments in materials chemistry because they offer diverse combinations of various distinct features in one single material. Their uniqueness has initiated an explosion ideas about potential material and applications. The definition of the hybrid materials is that inorganic components are bonded to organic moieties. The bond can be of various types of interaction such as covalent, coordinative, ionic, H-bonding and van-der Waals interactions (Figure 1.1). Therefore, the organic-inorganic hybrid nanomaterials basically compose two functional building blocks, the inorganic part provided as the architecture of the materials, and the organic part connecting special functionalities to the whole materials..[1].

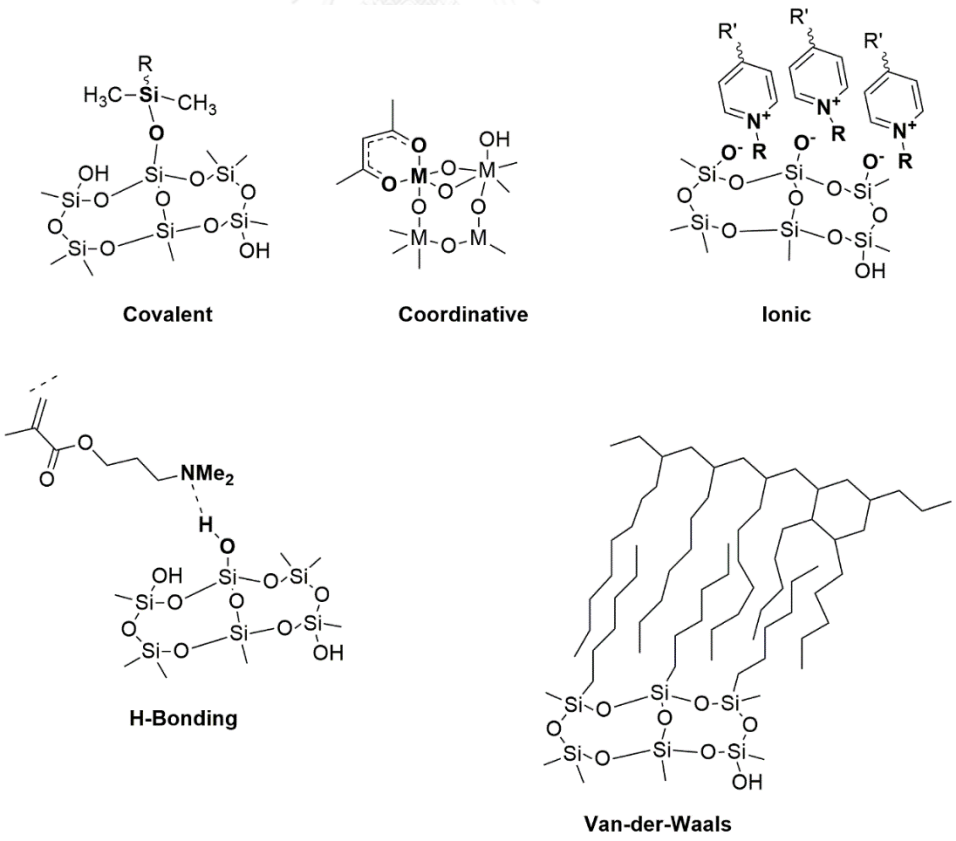

Figure 1.1 Interactions of organic applied in hybrid materials.

1.2 Literature review of hybrid nanomaterial for drug delivery

In 2009, Zhao *et al.*[2] studied the glucose - triggered controlled release of insulin and cyclic adenosine monophosphate using hybrid mesoporous silica nanoparticles as the carrier. In the experiment, the labeled gluconic acid - modified insulin proteins were decorated on the external surface of the silica particles while the cyclic adenosine monophosphate was absorbed into the mesopores. The results revealed that the loaded particles released both the gluconic acid and the cyclic adenosine monophosphate out of the mesoporous hosts through the introduction of monosaccharides such as glucose. In addition, the stimulation by the incorporation of glucose was found to enhance the efficiency of the insulin secretion from the pancreatic cells.

In 2012, Zhao *et al.*[3] succeeded in synthesizing the alginate/$CaCO_3$ hybrid nanoparticles through the coprecipitation method in order to deliver the plasmid gene (p53 plasmid) and the active drug (doxorubicin hydrochloride) to the HeLa cells. The particles exhibited high encapsulation efficiency of both drugs and plasmid. As the result, the co-loaded particles showed the highest inhibition of HeLa cell growth of 80%. The co-delivery of plasmid and drug showed higher cell growth inhibition activity than the delivery of plasmid and drug alone using the same system.

In 2013, Chen *et al.*[4] fabricated the ultrafine 10 – 30 nm silver/polymer (PDMAA) hybrid nanoparticles as an antibacterial agent by two synthesis routes, template and in-situ formation methods. Both preparation methods were proved successful in synthesizing the Ag/PDMAA hybrid nanoparticles. In particular, the in-situ formation method was developed to be used in large - scale processes and to reduce the uncontrollable factor including self-seeding nucleation of free Ag^+ in the solution from the template of synthesis route. The results demonstrated that the in-situ formation method yielded the nanoparticles of the similar size as those prepared via the template route. Moreover, the method was convenient route to gather the Ag/PDMAA hybrid nanoparticles. The product showed the high antibacterial performance.

1.3. The global statistic of cancer disease

Cancer is one of the major causes of death worldwide and it is rapidly becoming a global problem. The geographical distribution of cancer, which is categorized by organs inflicted, around the world is demonstrated below (Figure1.2). Generally, the most influential risk factors of cancer include age, genetic mutants (chemicals, heredity, irradiation etc.) drugs and alcoholism.

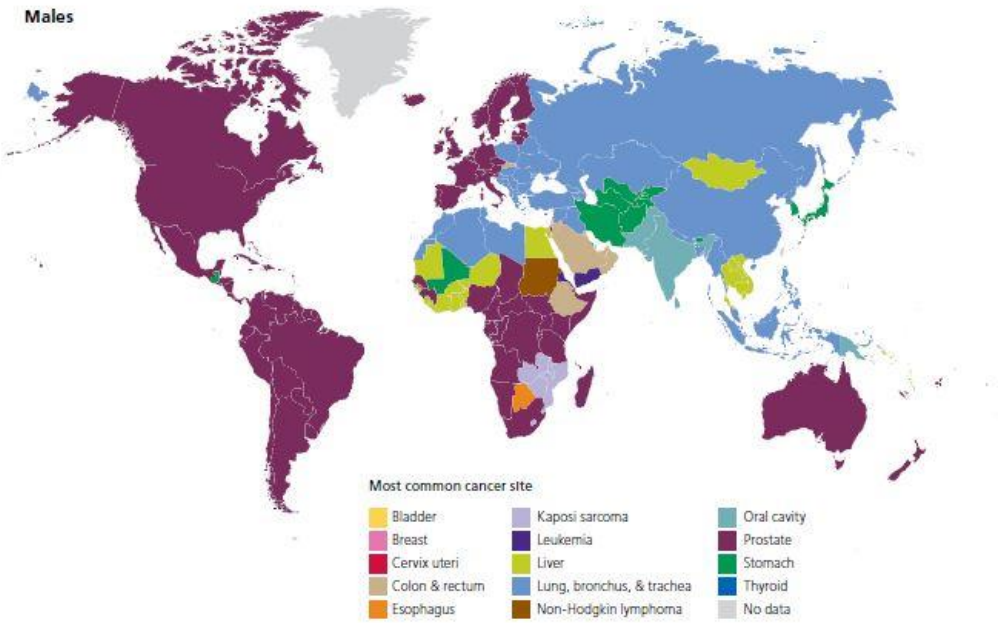

จุฬาลงกรณ์มหาวิทยาลัย
CHULALONGKORN UNIVERSITY

Figure 1.2 The distribution of common cancer around the world in male

Normally, the activity of anticancer agents depends on how the agents enter the cancer cells. In certain pathways, the agents taken up are trapped in endosomes. The agents are destroyed by acid and enzyme inside the endosome. As a result, the efficiency of the anticancer agents is low. In order to avoid this situation and improve the efficiency, one must strategize the scheme to provide the agents the escape route from the entrapment in the endosome. The followings are a copious amount of publications concerning this problem in drug delivery system.

1.4 Literature of application drug delivery system of cancer drugs

In 2007, Duan *et al*. [5] developed the cell-penetrating quantum dots (QDs) with the features of multivalents and endosome-disrupting surface coating (polyethlyeneimine). The quantum dots, which exhibited the luminescent property and adopted the core – shell structure, were then encapsulated by hyper branched copolymer ligand of polyethylene glycol (PEG) and polyethylenimine (PEI) through the ligand exchange mechanism. The result displayed the high efficiency of cellular uptake of polyethyleneimine - grafted polyethylene glycol (MW 14,100) quantum dots due to the ability of the particles to escape from the endosome. The size of quantum dots was reported around 21.8 nm.

In 2013, Lee *et al.*[6] developed the endo - lysosomal environmentally – responsive photodynamic nanocarriers, encapsulating with the hydrophoblic drug paclitaxel and the photosensitizer–mediated ELB disruption feature for effective cancer therapy. The self-assembled particles were formed by the interaction between photosensitizer and the polypeptide amphiphilic copolymer (methoxy polyethylene glycol-block-poly (β-benzyl-L-aspartic acid). The morphological characterisation displayed the spherical shape with the size of around 100 nm. Furthermore, the cellular uptake study revealed that these particles were capable of breaking through the endosomal entrapment. Upon laser irradiation, the photosensitizer absorbed the energy from the radiation to degrade the lipid membrane of endosome by lipid oxidation, which implied the instability of the endosomal compartment when exposed to the chemicals. Therefore, the role of the photosensitizer in the particles was to enhance anticancer activity when combined with the cancer drug in HeLa cell lines and drug -resistant HCT-8 cell lines.

In 2013, Sankaranarayanan *et al.*[7] prepared the logic gate nanoparticles with the aid of a newly synthesized random co-polymer platform. The polymeric nanoparticles contained pH - responsive moieties and the β-aminoester backbone moiety to provide the pH – triggered solubility. The study showed that the particles were able to encapsulate the small hydrophobic drugs and proteins. When the pH of the solution decreased and reached the endosomal level (pH=5), the particles

underwent the dramatic degradation because of fast hydrolysis reaction. Consequently, this phenomenon led to the increase in the osmotic pressure inside the endosome and the eventual release of the encapsulated chemicals to the cytoplasm.

In 2014, Wang *et al.* [8] was able to synthesize the pH-responsive polymeric nanocarriers of the derivatives of uronic acid (pH responsive moieties)/cholesterol succinate (hydrophobic moieties)–grafted pullulan. It was found that the particle morphology was spherical and the average size was approximately 150 nm. Under mildly acidic conditions at around 6.5, the particles were degraded and they subsequently released the anticancer drug, doxorubicin. In addition, the cellular uptake study investigated by the confocal microscopy demonstrated successful entry of the particles into to the cells and the MTT assay also revealed the enhancement of anticancer activity of the doxorubicin-encapsulating particles against MCF-7 cells.

1.5. Endocytosis pathway

1.5. Endocytosis pathway

Endocytosis [9] is the basic cellular uptake mechanism takes place at the cell membrane. The important character of endocytic pathway is the distinct membrane compartment that internalizes molecules from plasma membrane (early endosome). These compartments (endosomes) can then mature into late endosomes and lysosomes which increasing acidity and increasing presence of enzymes to degrade the internalized materials.

Early endosome [10] is the first state of endocytic pathway. Early endosome are frequently in the periphery of cell, and receive the most types of vesicles coming from the cell surface. Approximate pH of early endosome is 6.5.

Late endosomes [11] can mature into lysosomes. Late endosome are usually generated from early endosomes in endocytotic pathway, and phagosomes in the phagocytic pathway. Late endosome compose many membrane vesicles and characteristic proteins of lysosomes, including lysosomal membrane glycoproteins and acid hydrolase. Approximate pH of late endosome is 5.5.

Lysosomes [12] are the last compartment of the endocytic pathway. They are acidic part in the cell (approximately pH of 4.8). They are commonly considered as the important hydrolytic compartment of the cell. They have the high concentration of lysosomal membrane proteins and active lysosomal hydrolases. Lysosomes also use more than 40 types of the hydrolytic enzymes from endoplasmic reticulum and Golgi apparatus to degrade the internalized materials.

1.6 Zinc oxide nanoparticles

Zinc oxide is a white powder, water insoluble inorganic metal oxide, it has long been industrially used by numerous manufacturers including. In the health care industry; zinc oxide was added into the health care products to absorb UV radiation in the range from UVA (400-320 nm) to UVB (320-290 nm). In addition, the material has been declared non-toxic by FDA and is allowed to be used as a food and cosmetic additive. Apart from that, zinc oxide is also widely used in the electronic industry as the LED and the photocatalyst because of the wide direct band gap (3.37 eV or 375 nm at the room temperature) and large excitation energy (60 meV).

1.6.1 Crystal Structure of Zinc Oxide

The most stable structure of zinc oxide is the wurzite phase in which each oxygen atom is surrounded by four zinc atoms in the tetrahedral environment as shown in Figure 1.3. The physical properties of zinc oxide can be summarized in Table 1.1.

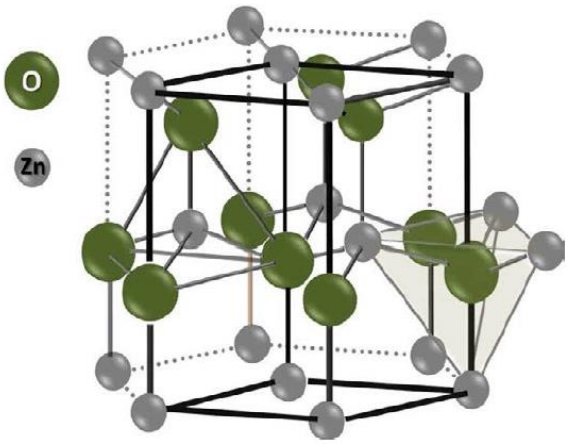

Figure 1.3 Crystal structure of zinc oxide
(http://www.edn.com/Home/PrintView?contentItemId=4391796)

Table1.1 Physical properties of ZnO

Properties	ZnO
Lattic parameters at 300 K	
- a_0(nm)	0.32495
- c_0(nm	0.52069
-c_0/a_0	1.602(1.633*)
Density (g/cm^3)	5.606
Stable phase at 300 K	Wurzite
Melting point (°C)	1975
Thermal conductivity ($Wcm^{-1}C^{-1}$)	0.6,1-1.2
Linear expansion coefficient(°C)	a_0 : 6.5 cm^3 x 10^{-6} c_0 : 3.0 cm^3 x 10^{-6}
Static dielectric constant	8.656
Refractive index	2.008
Band gap (RT)	3.370 eV
Band gap (4K)	3.437 eV
Excitation binding energy (meV)	60
Electron effective mass	0.24
Electron Hall mobility at 300K (cm^2/Vs)	200
Hole effective mass	0.59
Hole hall mobility at 300 K (cm^2/Vs)	5-50

1.6.2. Type of zinc oxide synthesis

Many publications were reported about the various kinds of routes of zinc oxide synthesis such as mechanochemicals [13, 14], precipitation [15-17], sol-gel method [18, 19], microemulsion method [19] and hydro/solvothermal methods [20, 21].

1.6.3 Hydro/Solvothermal synthesis

The hydro/solvothermal synthesis is a method that is employed to prepare a number of metal oxides. For example, Fe_2O_3, Cu_2O, and TiO_2 etc. In general, this environmentally – friendly method often produces highly – crystalline and high – purity products under the typical synthesis temperature ranging from 100 to 300 ^{o}C. Normally, the mechanism of zinc oxide formation comprises two steps. The first step involves the formation of hydroxide species (Figure 1.4A). The second step deals with the dehydration of water to form oxide particles. (Figure 1.4B) [19].

$$ZnCl_2 + 2NaOH \rightarrow Zn(OH)_2 + 2NaCl \quad (A)$$

$$Zn(OH)_2 \rightarrow ZnO + H_2O \quad (B)$$

Figure 1.4 The equation display the zinc oxide formation.

1.6.4. Solubility of zinc oxide in acid solution

Normally, zinc oxide is insoluble in water (pH=7) and various organic solvents. Zinc oxide is soluble in acid solution (pH of solution of lower than 4). The solvation of zinc oxide nanoparticles in acid solution is described as that zinc oxide can react with acid such as hydrochloric acid or sulfuric acid. The zinc ions in the system can form complex with anion species (Cl^- and SO_4^{2-}) from the acid. The product is the water soluble compounds ($ZnCl_2$ and $ZnSO_4$) [22, 23].

$$ZnO + HCl \rightarrow ZnCl_2 + H_2O \quad (A)$$

$$ZnO + H_2SO_4 \rightarrow ZnSO_4 + H_2O \quad (B)$$

Figure 1.5 The equation display the zinc oxide react with acid.

1.7. Application of zinc oxide in drug delivery.

In 2010, Barick *et al.* [24] was successful in preparing 100 – 300 nm mesoporous self-assembled zinc oxide nanoparticles using smaller 20 – 30 nm zinc oxide nanoparticles as a precursor. The obtained particles were loaded with doxorubicin anticancer drug and displayed the percentage of loading capability at 80% w/w. In addition, the cytotoxicity of the doxorubicin – loaded nanoparticles have the inhibitory effect on the cancer cell growth in HeLa cell lines.

In 2011, Muhammad *et al.* [25] was able to fabricate the well dispersed zinc oxide nanoparticles with the average particle size of 3 nm in aqueous solution by the ligand exchange method. This technique ensured the attachment of the amino group ($-NH_2$) on the surface of zinc oxide particles. In the experiment, the particles were modified by folic acid as a targeting compound and the encapsulation of doxorubicin. The observation indicated the better efficiency of the folic acid–modified nanoparticles over the non-modified counterpart.

In 2013, Zhang *et al.* [26] successfully prepared the zinc oxide hybrid nanoparticles using the non-toxic polymer polyacrylamide as a protective shell covering ZnO quantum dots (QDs). In vitro studies showed that after the polyacrylamide had been degraded, the ZnO QD core rapidly responded to low pH and was triggered to release DOX to destroy glioblastoma cells effectively

1.8. Anti-tumor activity of Zn ions in cancer cells

In 2002, Uzzo *et al.*[27] reported the potential of anticancer of zinc ions in PC-3 cell line through inhibition of NF- KB. Zinc ions reduce the expression of c-JAP2 gene.

In 2013, Yanf *et al.*[28] reported the mechanism of program of cancer cell death through apoptosis mechanism by zinc ions induction. The role of zinc ions have influence on the level of Smad2 and PIA2 proteins in cytoplasm are increased. The formation of Smad4/Smad2/PIAS1 architecture also is increased by the high of contents Smad2 and PIA2 proteins. The Smad4/Smad2/PIAS1 complex displays strong interacted at SBE1 and SBE3 region of $p21^{WAF1/Cip1}$promotor. Since, the interaction of

Smad4/Smad2/PIAS1 complex with $p21^{WAF1/Cip1}$ is increased expression of p21 gene and induction the cancer cell death by apoptosis.

1.9 Synergistic effect between zinc and tea polyphenol

In 2008, Sun *et al.* [29] conducted the study on the inhibition of cancer cell growth in PC-3 cell lines and it was found that the zinc ion – EGCG hybrid particles displayed the more pronounced synergistic effect of the anticancer activity with PC-3 cell lines than either EGCG or zinc ions alone.

In 2009, Yang *et al.* [30] reported that the Zn ion combined with EGCG could stimulate the production of cytochrome C from mitochondria to cytosol for the activation of caspase-9 enzyme. In addition, zinc ions could enhance the interaction between mitochondria and EGCG in PC-3.

จุฬาลงกรณ์มหาวิทยาลัย
Chulalongkorn University

1.10 Objective and scope of work

Objective

To synthesize the zinc oxide hybrid nanoparticles using 3 natural compounds (tea polyphenols extract, curcumin and α-mangostin) as shape controller, through hydrothermal synthesis.

Scope

The goal of this research can be concluded as follow:

1. Synthesis of the zinc oxide hybrid nanoparticles from natural substances including tea polyphenol extract (TP), curcumin (CM) and α-mangostin (MG) through hydro/solvothermal synthesis.
2. Characterization of TP-ZnO, CM-ZnO and MG-ZnO hybrid nanoparticles.
3. Evaluation of the loading capacity of the anticancer drug on TP-ZnO.
4. Cytotoxic study of the TP-ZnO nanoparticles particles and the anticancer drug–loaded particles in PC-3 cell line.
5. Cellular uptake study of TP-ZnO loaded nanoparticles.

จุฬาลงกรณ์มหาวิทยาลัย
Chulalongkorn University

CHAPTER II

EXPERIMENTAL

2.1 Materials and Chemicals

Solvent used in extraction of tea extracts was purchased from RCI Labscan (Bangkok, Thailand). Xanthone powder (±95% purity) extract was supplied by Welltechnology Company (Bangkok, Thailand). Curcumin was purchased from Acros Organic Company (Geel, Belgium) and, Oonlong tea leaves were purchased from Boon Rawd Farm, Chiang Rai, Thailand. Zinc chloride salts for analysis, triethlylamine reagent for synthesis, were supplied from Merck KGaA (Darmstadt, Geramany). Paclitaxel, doxorubicin hydrochloride, caffeine, zinc oxide nanoparticles (size < 100 nm) were purchased from Sigma-Aldrich ChemieGmbH (Steinheim, Germany). Epigallocatechin-3-gallate, gallic acid, epicatechin were purchased from Chemieliva Pharmaceutical and Chemical Company (Choqqing, China).

UV-Visible absorption spectrum was taken at 190-800 nm using UV-Visible spectrometer (OPTIZEN POP QX model, Korea) measuring in a quartz cell of 1 cm pathlength. Infrared spectrum was obtained on germanium reflection element using a Nicolet 6700 ATR-FT-IR spectrometer (Thermo Electron Corporation, Madison, WI, USA). Fluorescent images were acquired on Confocal Laser Scanning Microscope (Fluoview, FV10i-LIV, Tokyo, Japan). Size of particles was performed through scanning election microscope (JEOL, JSM-7610, Tokyo, Japan) and transmission electron microscope (JEOL JEM-2100, Tokyo, Japan). Functional group on the surface of particles was worked on x-ray photoelectron spectroscopy (AXIS-ULTRA DLD, Shimadzu/Kratos, Tokyo, Japan). Thermal analysis of particles was required thermo gravimetric analysis (Netzsch STA 449 F1, Geramany) and differential calorimetric analysis (Netzsch DSC 204 Phoenix, Germany). The crystallinity of particles was determined by the x-ray diffraction spectroscopic technique (Rigaku D/MAX-2200 Ultima-plus, Tokyo, Japan).

2.1.1 Media culture and chemical reagent for cell culture and treatment

Ham's F-12 Medium, fetal bovine serum, 100 mM sodium pyruvate, and HEPES (4-(2-hydroxyethyl)-1-piperazineethane sulfuric acid) (free acid 1 M solution (238.3 g/l)) were obtained from Hyclone (Utah, USA). Antibiotic-antimytotic solution were purchased from GIBCO BRL, Life Technologies Inc., NY, USA. 3-(4,5-Dimethyl-2-thiazolyl)-2,5-diphenyl-2-tetrazolium bromide or MTT was purchased from Sigma-Aldrich Chemical Co., St. Louis, MO, USA.

2.2 Preparation of tea polyphenol extract

Dried Oolong tea leaves (26 grams) were stirred with 300 ml of methanol at 55 ^{o}C. After 3 h, the mixture was cooled, filtered and evaporated under the reduced pressure at 50 ^{o}C. The crude methanol extract was partitioned by shaking in separation funnel with dichloromethane: methanol: water at the ratio 3:1:0.2 (v/v). The methanol layer was evaporated under low pressure at 55 ^{o}C using rotary evaporator to obtain tea polyphenol extract(5.04g).

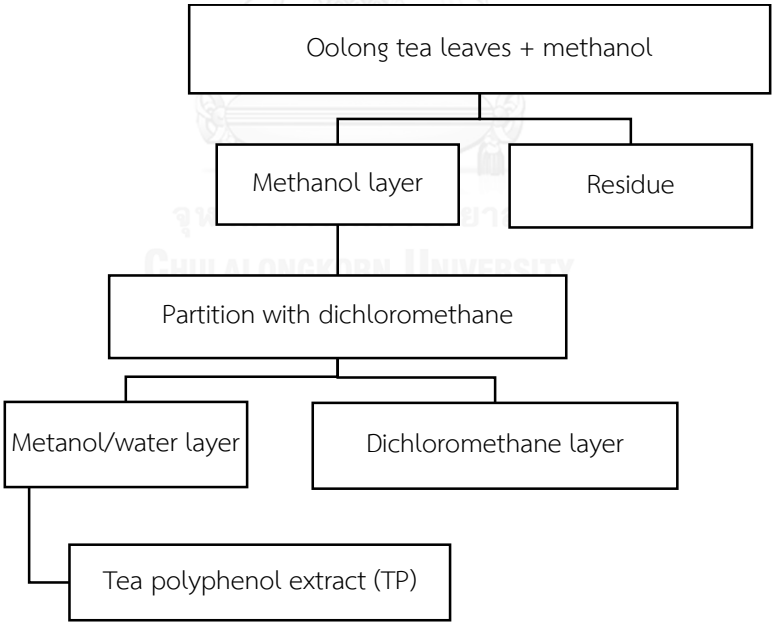

.

2.2.1 Quantification of each component in tea polyphenol extract by HPLC (High Performance Liquid Chromatography)

The crude methanol extract was analyzed by reverse phase high performance liquid chromatographic system (Water 1525 binary HPLC pump) coupled

to an UV-visible light detector (Water 2489). The column of this experiment was C18 reverse phase column (100 x 4.6 mm i.d.), packed with Hypersil C18 (Thermo Fisher Inc, Watham, Massachusetts, USA). The flow rate was set up at 0.7 ml/min and UV-detector was performed at 270 nm. Injection volume was 22 µl. Sample was dissolved in acetronitrile. The mobile phase composed the solution of formic acid 0.1% in Milli Q water (Solvent A) and acetronitrile (Solvent B). The gradient elution started at 95% solvent A and 5 % solvent B. Then, the content of solvent B was increased linearly to 15% within 14 min and maintained for 11 min. After that, the percentage of solvent B was increased to 35% within 28 min, and to 85% within 12 min. At the end, the column was re-equilibrated back to solvent B (95%) for 15 min before the next injection. Analysis was carried out in triplicate.

2.2.2. Calibration curve

The method development was concentrated on establishing the linear calibration curve for four components. The each standard solution containing gallic acid (30 – 70 µg/ml), caffeine (150-800 µg/ml), epigallocatechin-3-gallate (120-500 µg/ml) and epicatechin-3-gallate (40-120 µg/ml) was prepared in acetronitrile.

2.3 Synthesis of tea polyphenol-zinc oxide nanoparticles (TP-ZnO)

Zinc chloride (873 mg) and tea polyphenol extract (27mg) were dissolved in deionized water (50 mL), under vigorous stirring. Then, 1.25 M of sodium hydroxide solution was slowly dropwised for adjusting pH of solution to 7.3. The mixture was refluxed at 100 ^{o}C for 3 h. The solution was cooled and placed at the ambient temperature for 3 days. The mixture was centrifuged (15000 rpm for 15 min), the product was gathered and washed by deionized water. Finally, the pale yellow product was redispersed and subjected to further characterization.

2.3.1 Optimization on the amount of tea polyphenol used

To study the effect from amount of tea polyphenol on the shape of the obtained TP-zinc oxide nanoparticles, various amounts TP were studied (Table 2.1.).

Table2.1 Weight ratio between tea polyphenol and zinc chloride.

Sample	Tea polyphenol (mg)	Zinc chloride salts(mg)	Ratio TP:$ZnCl_2$
1	9.25	873	1:95
2	18.5	873	1:47
3	27	873	1:32
4	436.5	873	1:2
5	670	223	3:1
6	873	27	32:1

2.4 Synthesis of Curcumin-zinc oxide nanoparticles (CM-ZnO) and α-mangostin -zinc oxide nanoparticles (MG-ZnO)

Zinc chloride (873 mg) and curcumin (27 mg) were dissolved in mixture of 50% ethanol in deionized water under vigorous stirring. Then, triethylamine base was slowly dropped into the mixture to adjust the pH of the mixture solution to 7.3. The mixture was refluxed at 100 °C for 3 h. The solution was cooled and kept at the ambient temperature for 3 days. The mixture was centrifuged (15000 rpm for 15 min), the product (CM-ZnO) was gathered and washed by ethanol and deionized water. Finally, the pale yellow product was redispersed and subjected to further characterization.

The α-mangostin-zinc oxide nanoparticles (MG-ZnO) were synthesized similarly except that curcumin was replaced with α-mangostin.

2.5 Loading of drugs on TP-ZnO nanoparticles

The doxorubicin and paclitaxel as two drugs were selected as model drug in this experiment.

The TP-ZnO particles (2000 μg/ml) were blended with doxorubicin (200 μg/ml) in water (total volume 1000 μl) and kept in dark for 24 h at room temperature. The mixture was centrifuged (13500 rpm, 10 min). The percentage of encapsulation efficiency eq. (1) and loading capacity eq. (2) was determined amount of unloaded drug through supernatant by UV-Visible spectroscopy at maximum absorption wavelength 230 nm by calibration curve of drug.

$$\%Encapsulation\ efficiency = \frac{Weight\ of\ Dox\ found\ in\ paritcles}{Weight\ of\ Initially\ used} \times 100 \quad \text{eq.(1)}$$

$$\%Loading = \frac{Weight\ of\ Dox\ found\ in\ paritcles}{Weight\ of\ Dox{-}loaded\ particles} \times 100 \quad \text{eq. (2)}$$

The paclitaxel loading onto TP-ZnO was performed similarly except that solution of doxorubicin in water replaced with 40% of ethanolic aqueous solution.

2.6 In Vitro antitumor assay

Paclitaxel loaded TP-ZnO, Doxorubicin loaded TP-ZnO, unloaded TP-ZnO, ZnO nanoparticles, unloaded paclitaxel in 40% ethanol and doxorubicin were test with PC-3 cells.

2.6.1 Cell culture

PC-3 human prostatic adenocarcinoma cell lines was obtained from American Type Culture Collection (ATCC, RockVille, MD, USA). The PC-3 cells was treated in F-12k Medium supplemented with 10% (v/v) fetal bovine serum and 100 U/ml penicillin, 100µg/ml streptomycin and 125 ng/ml amphotericin B, at 37 °C in humidified atmosphere of 5% CO_2.

2.6.2 Cell viability assay

Cell viability was calculated by MTT assay with some modification. Briefly, cell suspensions in completed medium were seeded at $1x10^4$ cells in 96-well plates (100µl/well) and incubated at 37 °C in humidified atmosphere of 5% CO_2. After 24 h, additional medium (100µl) containing sample was added to each well, followed by further incubation for 72 h. Then, the wells were replaced and incubated with fresh medium containing of 3-(4,5-dimethylthiazol-2-yl)-2,5-diphenyltetrazolium bromide (MTT reagent) 0.5 mg/ml for 2 h at 37 °C. Finally, the media were removed and 100 µl of DMSO was added to each well. The absorbance was measured at 550 nm in microplate reader. Usually, the MTT reagent is yellow color with the maximum absorption wavelength of 650 nm. The incubation of MTT with metabolically active cells, MTT will be reduced into insoluble purple formazan dye crystals which absorbs the light at 550 nm. The number of viable cells can be determined from the difference

of absorbance at 550 nm. The experiments were performed in triplicate. The results were reported as percent of viability.

2.7 Cellular uptake of loaded DOX-TP-ZnO

The uptake of DOX-TP-ZnO was investigated on PC-3 human prostatic adenocarcinoma cells. The PC-3 cells were grown in F-12k medium, 10% (v/v) fetal bovine serum and 100 U/ml penicillin, 100µg/ml streptomycin and 125 ng/ml amphotericin B at 37°C in humidified atmosphere of 5% CO_2.

The PC-3 cells ($8x10^4$ cell) were seeded into 8-well plate (Lab-Tek II Chambered Coverglass, sNUNC, NY, USA) in 200 µl/well with media culture and allowed to adhere overnight. The 20 µl (2 µl/10,000 cell) of early endosome RFP (Molecular probes, Life technologies, USA) were treated with PC-3 cell ($8x10^4$ cells/well) and incubation at 37 °C, 5% CO_2 for 16 h. Then, 75 µl of 2 µM of lysotracker deep red in 0.1 mM phosphate buffer saline (Molecular probes, Life technologies, USA) and 3 µl of 30 µM zinquin ester (Sigma-Aldrich Chemical Co., St. Louis, MO, USA.) solution in DMSO (as zinc ion tracking agent) were added to each wells and incubation for 20 min. After that, cells were treated with DOX-TP-ZnO (100 µl, 1000 ppm), and incubated at 37 °C in a CO_2 incubator and monitored under confocal fluorescence microscope (Olympus, Fluoview, FV10i-LIV). The excitation of zinquin, doxorubin, early endosome RFP and lysotracker deep red were performed with laser 405, 473, 559, 635 nm, and emission spectra were collected using the wavelength range on 450, 570, 584, and 658 nm, respectively. The image data were analyzed through FV10-ASW software. Image indicating locations of DOX-TP-ZnO was then constructed using the obtained resolved signal.

CHAPTER III

RESULTS AND DISCUSSION

The aim of this work is to synthesize tea polyphenol-zinc oxide hybrid nanoparticles (TP-ZnO) as a carrier to deliver anti-cancer drug into PC-3 cancer cell line. This work also illustrated hybrid zinc oxide nanoparticle platform with another natural compounds, e.g., curcumin (CM-ZnO) and α-mangostin (MG-ZnO).

Therefore, the work includes the preparation of TP-ZnO, CM-ZnO and MG-ZnO hybrid nanoparticles, and cytotocixity evaluation and cellular uptake studies of the obtained particles.

The work started with the extraction of tea polyphenol from the tea leaves. The work, thus involves also the characterization of the obtained extract.

3.1 Quantification of each component in tea polyphenol extract by HPLC (High Performance Liquid Chromatography)

The extraction of tea leaves gave us 3.375 g of the extract from 15 g of dry tea leaves. The HPLC analysis was used for the quantitation of contents in the obtained tea polyphenol extract. The chromatogram showed four major peaks (Figure 3.1) at retention times 2.6, 17.0, 24.6, 31.6 minutes, labeled as A, B, C and D in figure 3.1, corresponded with the retention times of the standard gallic acid, caffeine, epigallocatechin-3-gallate and epicatechin-3-gallate, respectively.

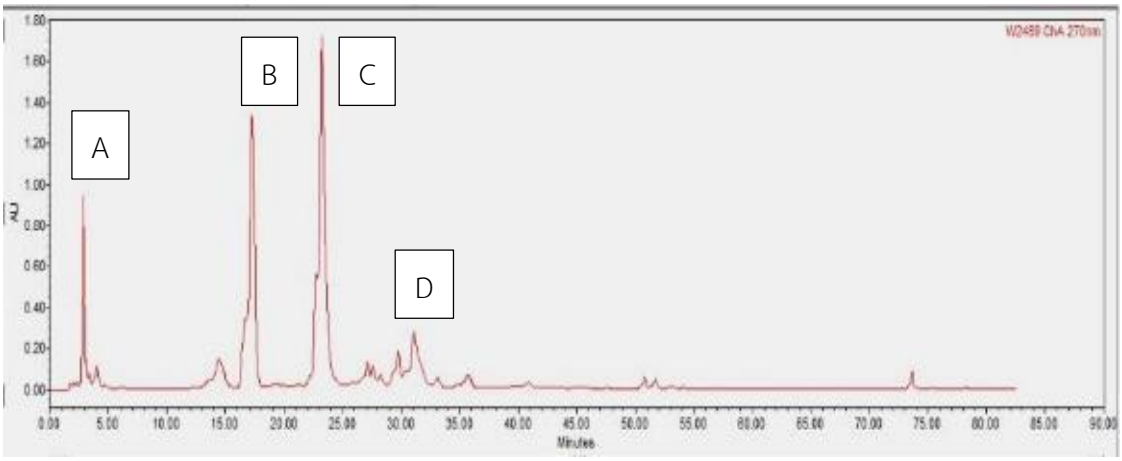

Figure 3.1 Chromatogram of tea polyphenol extract (TP).

Noted that the calibration curve was obtained by plotting peak area versus concentration of each standard (gallic acid at 30 – 70 μg/ml, caffeine at 150-800 μg/ml, epicgallocatechin-3-gallate at 120-500 μg/ml and epicatechin-3-gallate at 40-120 μg/ml, respectively). The correlation coefficients for all standard compounds were greater than 0.99, suggesting good linearity for the calibration curves of the four standard compounds. Table 3.1 shows the contents of the four major components in crude methanol extract. EGCG was the major component (24.48% w/w), followed with caffeine at 3.15% w/w, and then gallic acid and epicatechin-3-gallate at 1.89% w/w and 0.45% w/w, respectively.

Table 3.1 Contents of the four major components in tea polyphenol extract.

Contents	**Retention time (min)**	**Concentration of Content (%w/w)**
Gallic acid (GA)	2.6	0.45
Caffeine (C)	17.0	3.15
Epigallocatechin-3-gallate (EGCG)	24.6	24.48
Epicatechin-3-gallate (ECG)	31.6	1.89

จุฬาลงกรณ์มหาวิทยาลัย
Chulalongkorn University

3.2 Synthesis of tea polyphenol-zinc oxide nanoparticles (TP-ZnO)

This study involves the synthesis of tea polyphenol-zinc oxide hybrid nanoparticles by hydrothermal synthesis (Scheme 3.1). In the aqueous system, tea polyphenol was first mixed with zinc ions (added as zinc chloride). When sodium hydroxide was dropped, the mixture turned into slurry. After reflux, the mixture appeared as milky pale brown suspension. We speculated that the complexation between tea polyphenol and zinc hydroxide ions first occurred and followed with the dehydration of zinc hydroxide into zinc oxide, resulting in TP-ZnO hybrid nanoparticles.

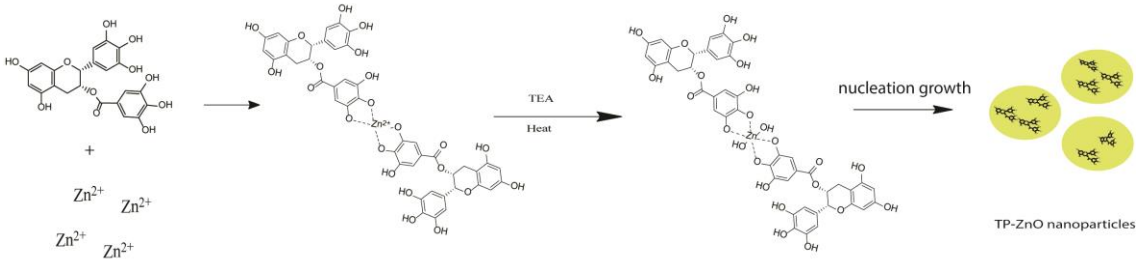

Scheme 3.1 Synthesis of TP-ZnO nanoparticles through hydrothermal synthesis by nucleation of zinc oxide nucleus.

3.2.1 Optimization on the amount of tea polyphenol extract used

We studied the effects of the amount of tea polyphenol used in the preparation of tea polyphenol-zinc oxide nanoparticles, on the morphology of the obtained products.

The morphology of all products were characterized by scanning electron microscopy (Table 3.2). It is obvious that the amount of TP influences morphology of the product. The TP-ZnO spherical nanoparticles could be obtained at the TP: $ZnCl_2$ ratio of 1:32 (w/w). Dried sizes of TP-ZnO nanoparticles obtained at this material ratio, estimated from the SEM picture, was 16.46 ±5.25 nm. When the weight of tea polyphenol decreased to 1:47 (w/w), the size of the obtained particles increased to 66 ± 14.9 nm. Further decrease in the amount of tea polyphenol resulted in product with no specific nanostructural morphology. On the contrary, when the amount of tea polyphenol increased to 1:2 (polyphenol to $ZnCl_2$, w/w), the product exhibited sheet and plate-like structure. When the amount of tea polyphenol was further increased

(3:1 and 32:1), no particular nano or microstructral morphology of the product could be observed. We then concentrated our preparation on ratio of 1:32 (w/w) for further experiments.

Table 3.2 SEM results of prepared tea polyphenol-zinc oxide nanoparticles (TP-ZnO)

	Ratio TP:$ZnCl_2$	Magnification	SEM photograph
1	1:95	20,000x	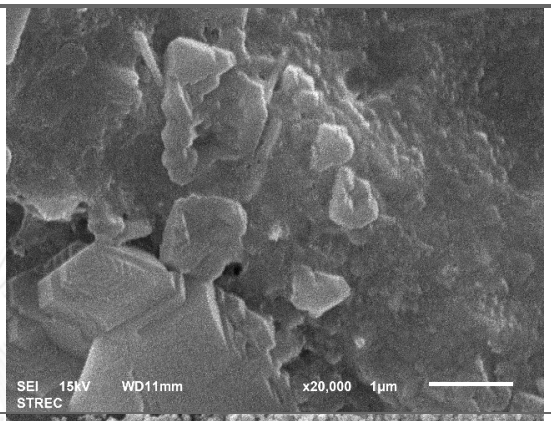
2	1:47	20,000x	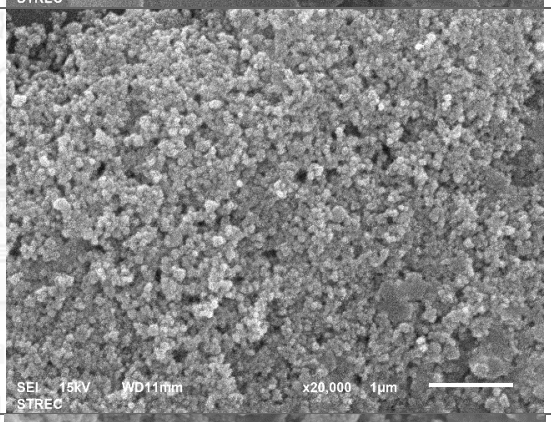
3	**1:32**	**50,000x**	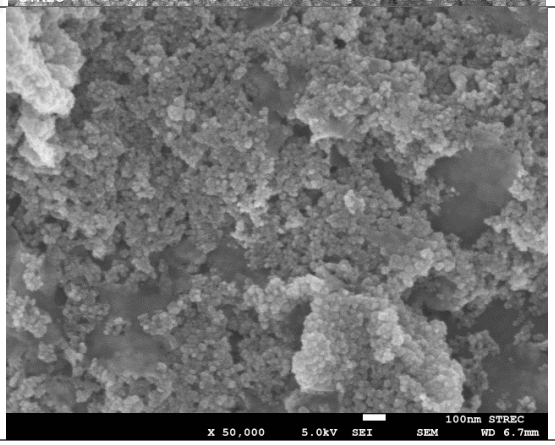

	Ratio TP:$ZnCl_2$	Magnification	SEM photograph
4	1:2	20,000x	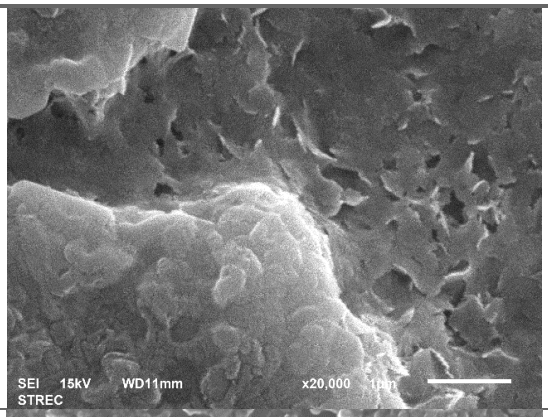
5	3:1	50,000x	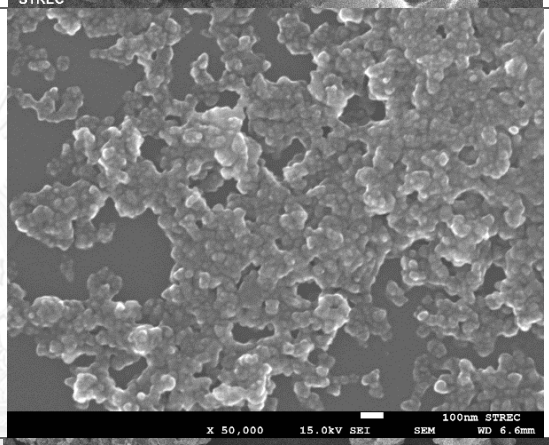
6	32:1	10,000x	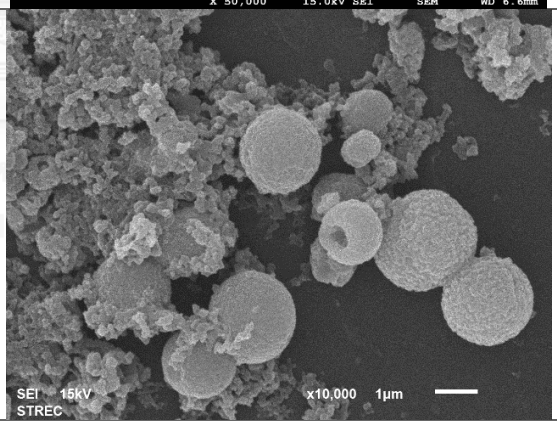

จุฬาลงกรณ์มหาวิทยาลัย
Chulalongkorn University

3.3 Synthesis of Curcumin-zinc oxide nanoparticles (CM-ZnO) and α-mangostin -zinc oxide nanoparticles (MG-ZnO)

This study also involves the synthesis of curcumin-zinc oxide hybrid nanoparticles by hydrothermal synthesis (Scheme 3.2). In the ethanolic solution system, curcumin was first blended with zinc ions (added as zinc chloride). When triethylamine was dropped, the mixture turned into slurry. After reflux, the mixture appeared as milky yellowish suspension. We speculated that the complexation between curcumin and zinc hydroxide ions first occurred and followed with the dehydration of zinc hydroxide into zinc oxide, resulting in CM-ZnO hybrid nanoparticles.

The α-mangostin-zinc oxide nanoparticles (MG-ZnO) were synthesized similarly except that curcumin was replaced with α-mangostin.

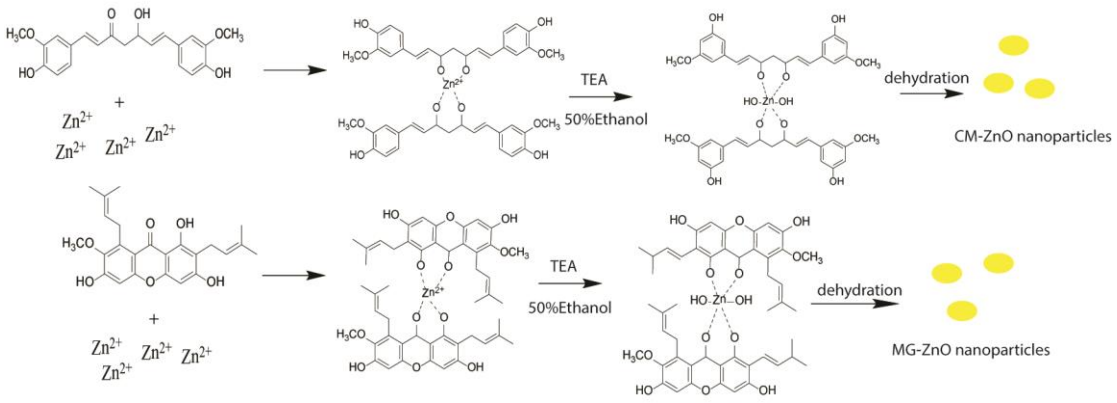

Scheme 3.2 Synthesis of CM-ZnO and MG-ZnO nanoparticles through hydrothermal synthesis by the nucleation of zinc oxide nucleus

3.4 Morphology of all products

The morphology of all products were characterized through scanning electron microscopy (Figure 3.2) and transmission electron microscopy (Figure 3.3). It is clear that the type of natural product used influences morphology of the product.

As shown above that the dried sizes of TP-ZnO nanoparticles obtained at this material ratio, estimated from the SEM picture, was 16.5 ±5.3 nm (Figure 3.2C), in contrast, the nanostructural morphology of MG-ZnO was the square prism (TEM images, Figure 3.3 A). The size and dimension of dried product was performed by SEM (Figure 3.2A) and TEM (Figure 3.3A) images and the product architecture as shown Figure 3.4A. The CM-ZnO nanoparticles exhibited the hexagonal rod shape. The size and dimension of CM-ZnO was performed by SEM (Figure 3.2B) and TEM (Figure 3.3B) images. The size and dimension of CM-ZnO display the product architecture as shown in the Figure 3.4B.

The organic compounds in each of nanoparticles were extracted by solvent extraction, and quantified through UV-Visible spectroscopy with the aid of corresponding calibration curve. Concentration ranges and wavelength used for the analysis of each natural organic materials were as followed: tea polyphenol (λ_{max} = 270 nm) 1-10 µg/ml curcumin (λ_{max}= 425 nm) 1-10 µg/ml and α-Mangostin (λ_{max} = 202 nm) 2 – 50 µg/ml.

Chulalongkorn University

Table 3.2 shows the amount of each organic matter in the particles. The TP-ZnO nanoparticles contain the highest organic matter (tea polyphenol) in the particles at 0.97±0.018 %w/w, followed with the α-mangostin (MG) in MG-ZnO nanoparticles at 0.74 ± 0.027 %w/w and curcumin in CM-ZnO nanoparticles at 0.066 ± 0.011 %w/w.

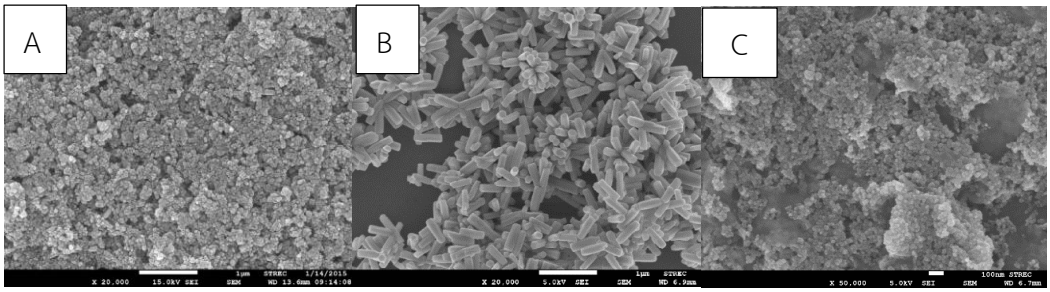

Figure 3.2 SEM results of (A) α-Mangostin-zinc oxide (MG-ZnO), (B) Curcumin-zinc oxide (CM-ZnO) and (C) Tea polyphenol zinc oxide (TP-ZnO) nanoparticles.

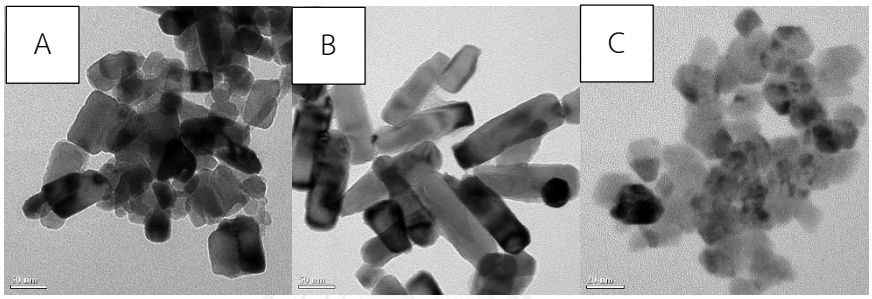

Figure 3.3 TEM micrographs of (A) Mangostin-zinc oxide (MG-ZnO), (B) Curcumin-zinc oxide (CM-ZnO) and (C) Tea polyphenol zinc oxide (TP-ZnO) nanoparticles.

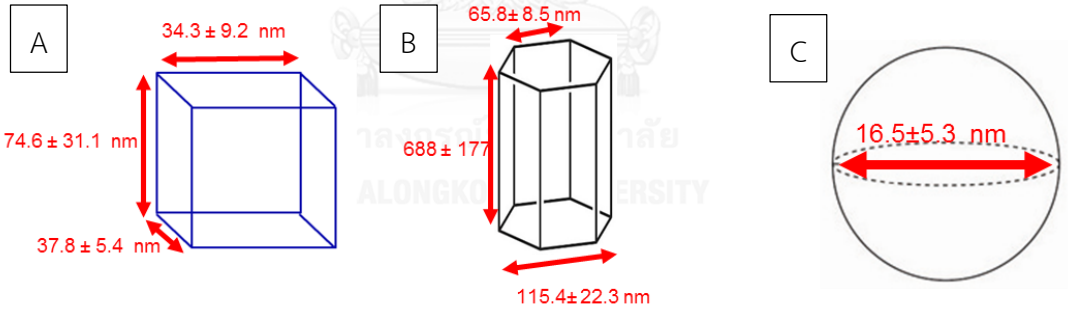

Figure 3.4 The dimension and of each product (A) Mangostin-zinc oxide (MG-ZnO), (B) Curcumin-zinc oxide (CM-ZnO) and (C) Tea polyphenol zinc oxide (TP-ZnO) nanoparticles.

Table 3.3 The amount of organic matter in each nanoparticles

Particles	Natural compounds	Amount of organic materials (%w/w)
TP-ZnO	Tea polyphenol	0.97 ± 0.018
CM-ZnO	Curcumin	0.066 ± 0.011
MG-ZnO	α-mangostin	0.74 ± 0.027

จุฬาลงกรณ์มหาวิทยาลัย
Chulalongkorn University

3.5 Crystal structure analysis

The crystallographic structures of all products were determined using X-ray powder diffraction (XRD) analysis. The XRD patterns of all products (TP-ZnO (red line), MG-ZnO (blue line) and CM-ZnO (green line)) indicated standard zinc oxide crystal structure (black line). As the results, the the ZnO crystal structure in the TP-ZnO nanospheres, MG-ZnO square prism and CM-ZnO hexagonal prism were confirmed.

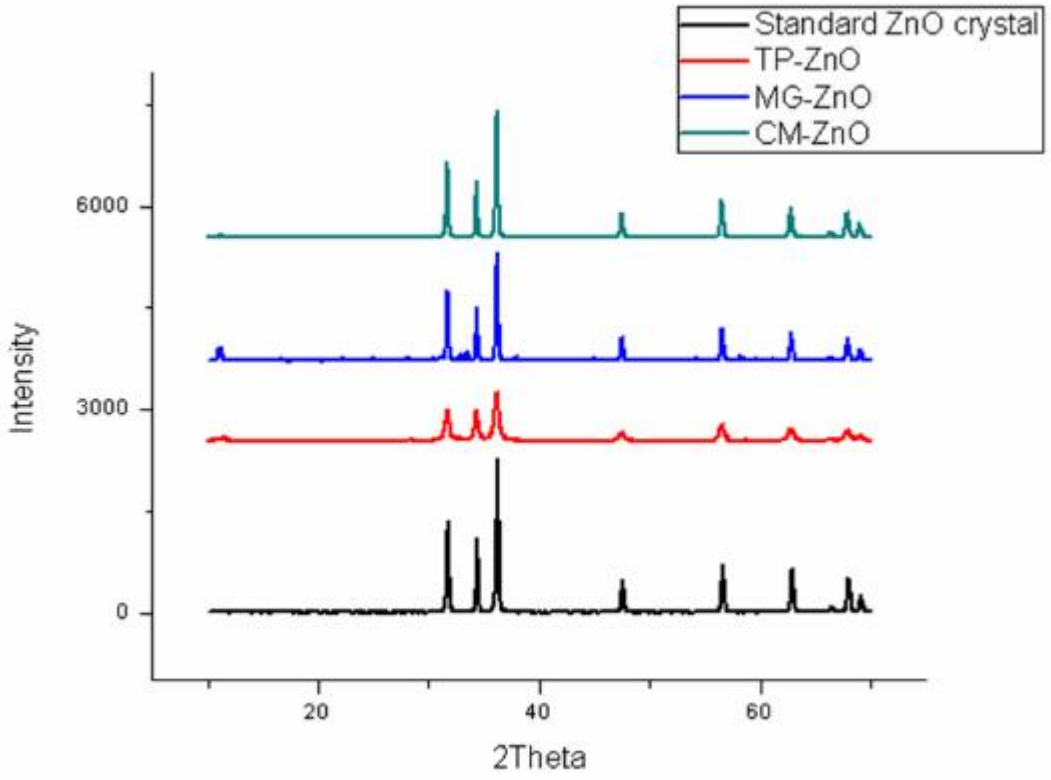

Figure 3.5 X-ray diffraction patterns of TP-ZnO (red line), MG-ZnO (blue line), CM-ZnO (green line) and standard ZnO crystal (black line).

3.6 Chemicals interaction of organic matters with zinc oxide in the nanoparticles

The existing of organic matters in TP-ZnO, CM-ZnO and MG-ZnO hybrid nanoparticles were confirmed by FT-IR and UV-spectroscopy. The FT-IR spectrum of TP-ZnO nanoparticles (Figure 3.6, red line) showed C=C stretching at approximately 1588.48 cm^{-1} (benzene ring of tea polyphenol), O-H stretching at 1384.02 cm^{-1} (hydroxyl group from tea polyphenol) and C-O stretching at 1043.24 cm^{-1}. The wavenumber of tea polyphenol in particles exhibited the IR absorption peaks at the lower frequency than free tea polyphenols (Figure 3.5, blue line). Since, zinc oxide was electron deficient, therefore, the electron rich substructures of the tea polyphenol, e.g., C=C (1604.71 cm^{-1}), -OH (1450.21 cm^{-1}) and C-O (1140 cm^{-1}) could donate electron to zinc oxide. The complexation of these electron rich functional groups to the electron deficient ZnO resulted in the weakening of those original bonds, therefore, their vibrational frequencies were shifted to lower numbers.

The FT-IR spectra of MG-ZnO (Figure 3.7, red line) nanoparticles showed the C=C stretching at approximately 1529.86 cm^{-1}(benzene ring or allylic group from **α**-mangostin), -OH stretching at 1216.78 cm^{-1} (hydroxyl group from **α**-mangostin) and C-O stretching at 952.91 cm^{-1}.

The FT-IR spectra of CM-ZnO (Figure 3.8, red line) nanoparticles showed the C=C stretching at approximately 1591.92 cm^{-1} (benzene ring from curcumin) and C-O stretching at 1034.34 cm^{-1}.

The wavenumber of **α**-mangostin and curcumin in particles exhibited the IR absorption peaks at the lower frequency than free **α**-mangostin (Figure 3.7, light blue line) and curcumin (Figure 3.8, green line). Usually, the zinc oxide nanoparticles display the electron deficient, the electron rich group such as the C=C (1606.83 cm^{-1}), –OH (1276 cm^{-1}) from **α**-mangostin and C=C (1622.56 cm^{-1}) and C-O (1019.65 cm^{-1}) could donate to zinc oxide. Thus, the complexation of the electron rich functional groups to the electron deficient ZnO resulted in the weakening of those original bonds, therefore, their vibrational frequencies were shifted to lower numbers.

In addition, the FT-IR of the mixture between zinc oxide and each natural compound (tea polyphenol (TP), curcumin (CM), and α-mangostin(MG)) exhibited the same IR signals (Figure 3.9) of all natural compounds as with free natural compounds. Since, the result display non-interaction of natural compound with zinc oxide nanoparticles. We conclude that the hybrid zinc oxide nanoparticles cannot be fabricated from blending of natural compounds with zinc oxide nanoparticles.

จุฬาลงกรณ์มหาวิทยาลัย
Chulalongkorn University

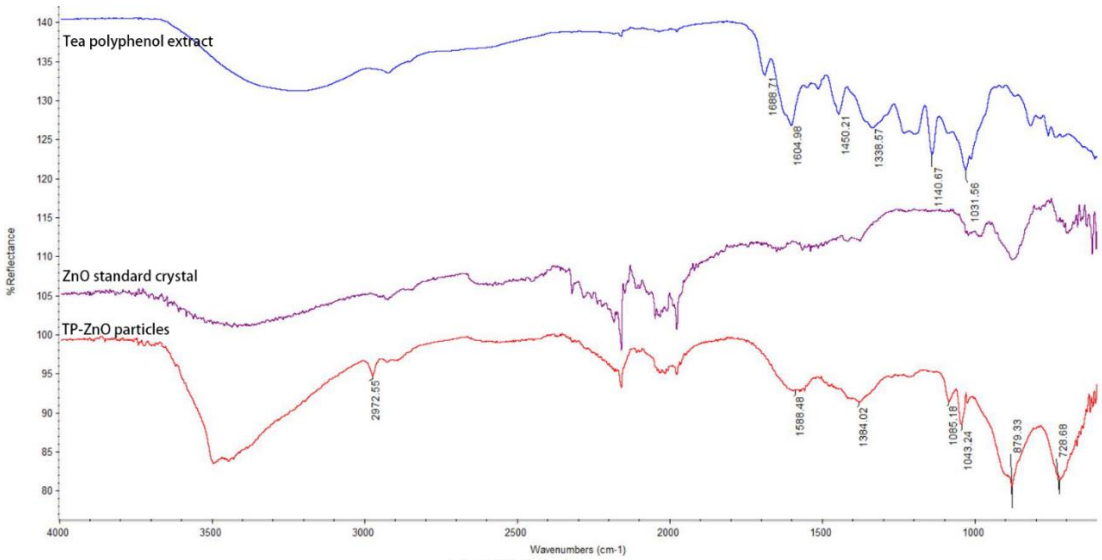

Figure 3.6 FT-IR spectra of TP-ZnO nanoparticles (red line), tea polyphenol extract (blue line) and zinc oxide crystal standard (purple line).

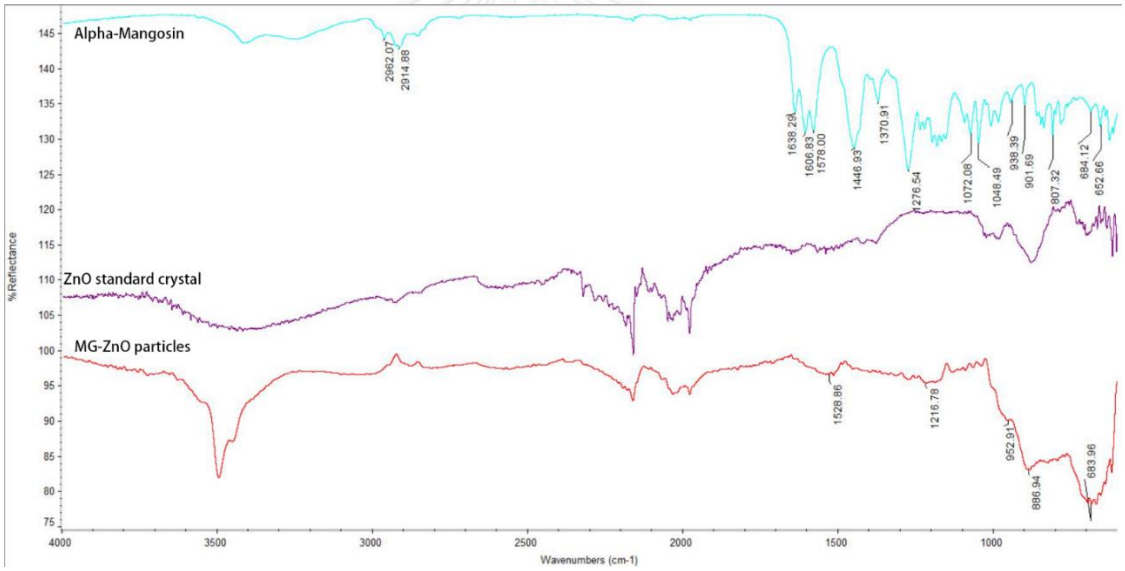

Figure 3.7 FT-IR spectra of MG-ZnO nanoparticles (red line), α-mangostin (light blue line) and zinc oxide crystal standard (purple line).

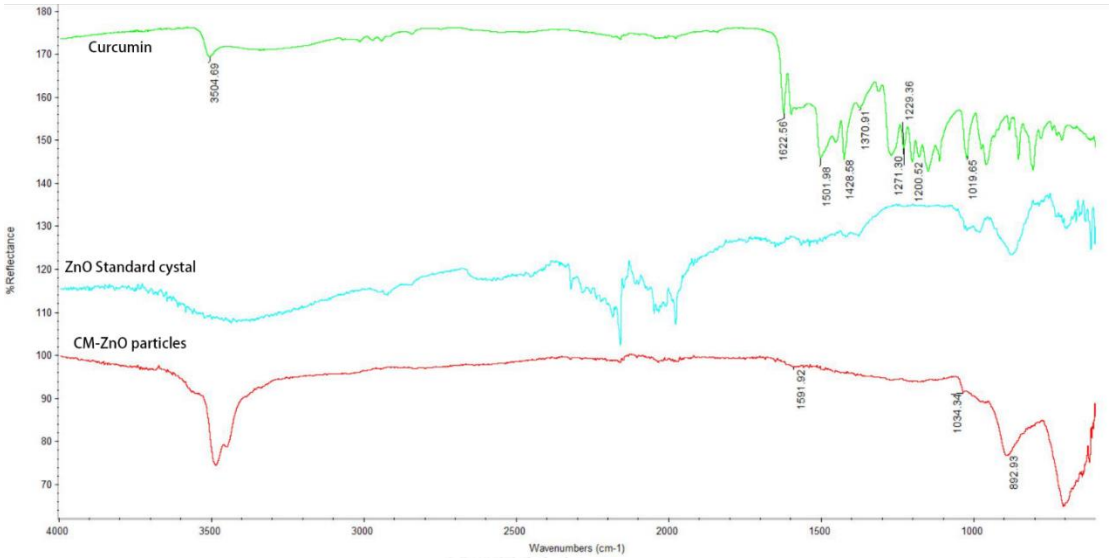

Figure 3.8 FT-IR spectra of CM-ZnO nanoparticles (red line), curcumin (green line) and zinc oxide crystal standard (purple line).

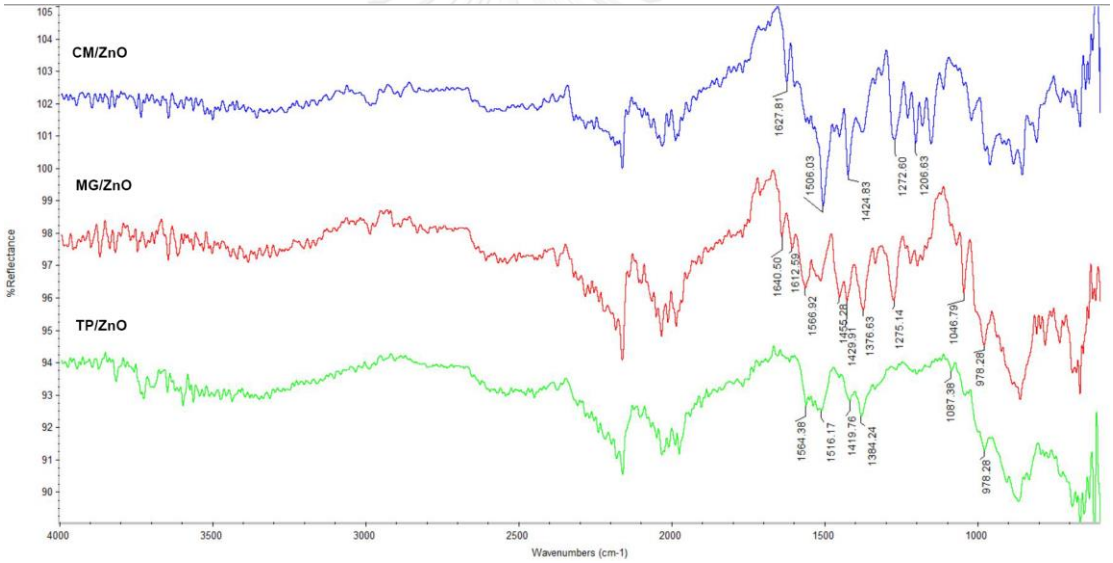

Figure 3.9 FT-IR spectra of composite of curcumin/ZnO (CM/ZnO,blue line), **α**-mangostin/ZnO(MG/ZnO, red line) and teapolyphenol/ZnO(TP/ZnO, green line) nanoparticles

3.7 The organic matters inside zinc oxide nanoparticles

UV spectroscopic analysis was performed to identify the natural compound in the particles. The experiments were performed by each particle was solvated in the acidic aqueous solution. The TP-ZnO nanoparticles was solvated in the acidic aqueous solution. The turbidity of suspension TP-ZnO nanoparticles gradually decrease and turn to clear solution at pH=4.5. The mixture was investigated the uv-absorption peak of tea polyphenol extract.

The CM-ZnO and MG-ZnO nanoparticles were dissolved in the acid solution. All mixture were extracted by organic solvent such as ethyl acetate. The UV spectroscopy were used to detect the UV characteristic absorption wavelength of natural compounds in particles as shown in the UV absorption spectrum.

Maximum wavelength of the tea polyphenol from TP-ZnO nanoparticles (Figure 3.9, blue line) was blue-shifted from these of the corresponding original materials. The blue-shift phenomenon implied less conjugation in both compounds structure resulting from the metal (electron deficiency group) complex with conjugation of carbon (electron donating group).

The maximum wavelength of curcumin extract from CM-ZnO nanoparticles (Figure 3.10, green line) exhibited the UV absorption peak at 405 nm. The characteristic of UV absorption of free curcumin (Figure 3.10, yellow line) could not be observed in UV-Vis spectra. Thus, curcumin from CM-ZnO displays the transformation of chemical structure of curcumin from CM-ZnO nanoparticles. We speculated that curcumin in CM-ZnO does not existing the same structure of free curcumin.

The **α**-mangostin extract from MG-ZnO nanoparticles (Figure 3.11, red line) showed the UV-visible absorption spectrum at 202, 246, 262 and 318 nm. This spectrum of the extract exhibited the same wavelength with free **α**-mangostin. Thus, this result could conclude existing of **α**-mangostin in the MG-ZnO nanoparticles.

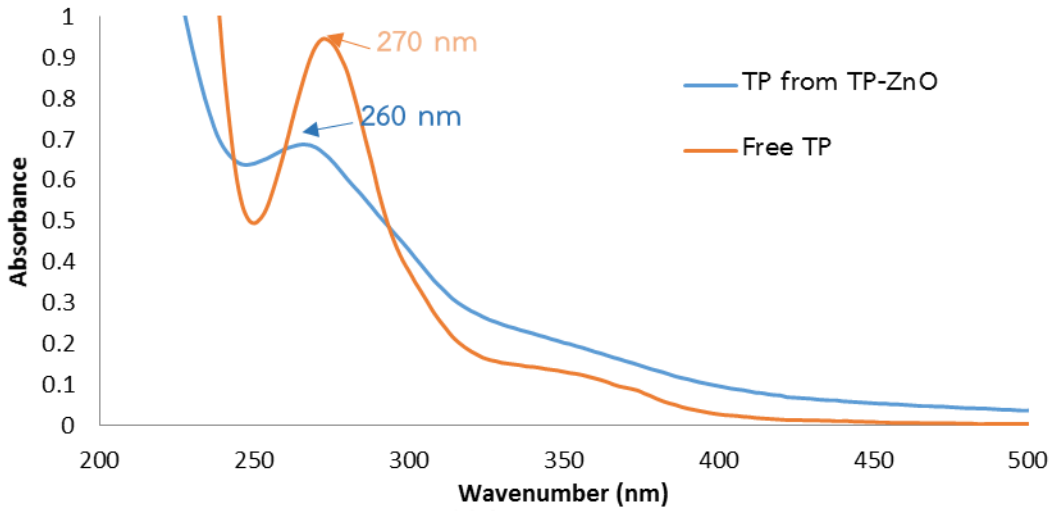

Figure 3.10 UV absorption spectra of free tea polyphenol (TP, orange line) and TP from TP-ZnO (blue line).

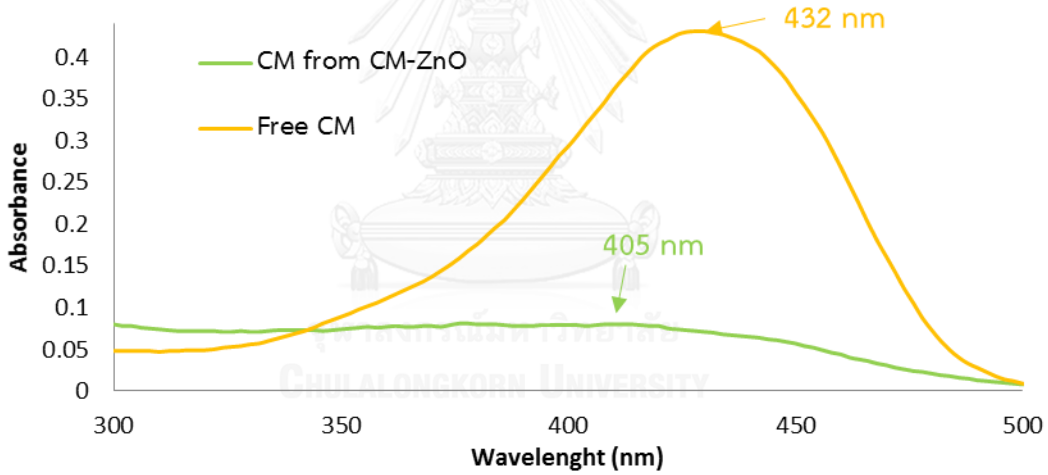

Figure 3.11 UV absorption spectra of free curcumin (CM, yellow line) and CM from CM-ZnO (green line).

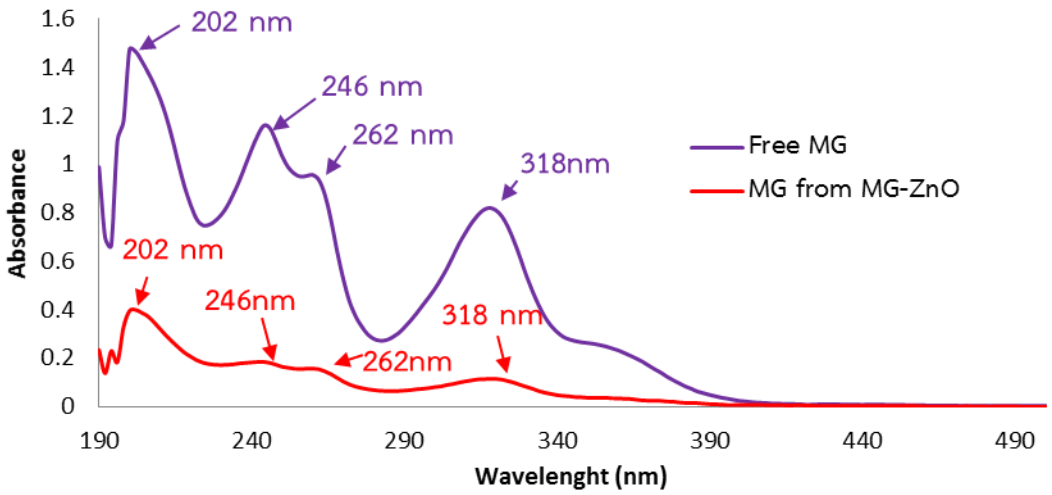

Figure 3.12 UV absorption spectra of free α-mangostin (MG, red line) and MG from MG-ZnO (purple line).

จุฬาลงกรณ์มหาวิทยาลัย
Chulalongkorn University

3.8 Interactions between the natural compounds (tea polyphenol, curcumin and α-mangostin) and the ZnO crystals within the hybrid nanoparticles.

The interaction of the organic molecules (tea polyphenol, curcumin and α-mangostin) and the ZnO crystals in the obtained hybrid nanoparticles was also investigated by thermal gravimetric analysis (TGA) (Figures 3.12-3.14) and differential scanning calorimetric analysis (DSC) (Figures 3.15-3.17). In the TGA thermograms, the usual characteristic weight loss (TG) peaks of the organic matters (tea polyphenol at 177°C, curcumin at 174 °C, and α-mangostin at 189°C) could not be observed in particles. Instead, the weight loss peaks at 201.7°C, 231.1°C and 395.6°C from TP-ZnO, CM-ZnO and MG-ZnO nanoparticles, were observed. Since these peaks were not observed in the ZnO standard thermogram, we speculated that they belonged to the organic matters within the particles. This shift of the weight loss from 177°C, 174°C and 189°C of the free natural compounds to 201.7°C, 231.1°C and 395.6°C after being incorporated within the TP-ZnO, CM-ZnO and MG-ZnO nanoparticles, indicated strong interaction between the organic matters and the zinc oxide crystals.

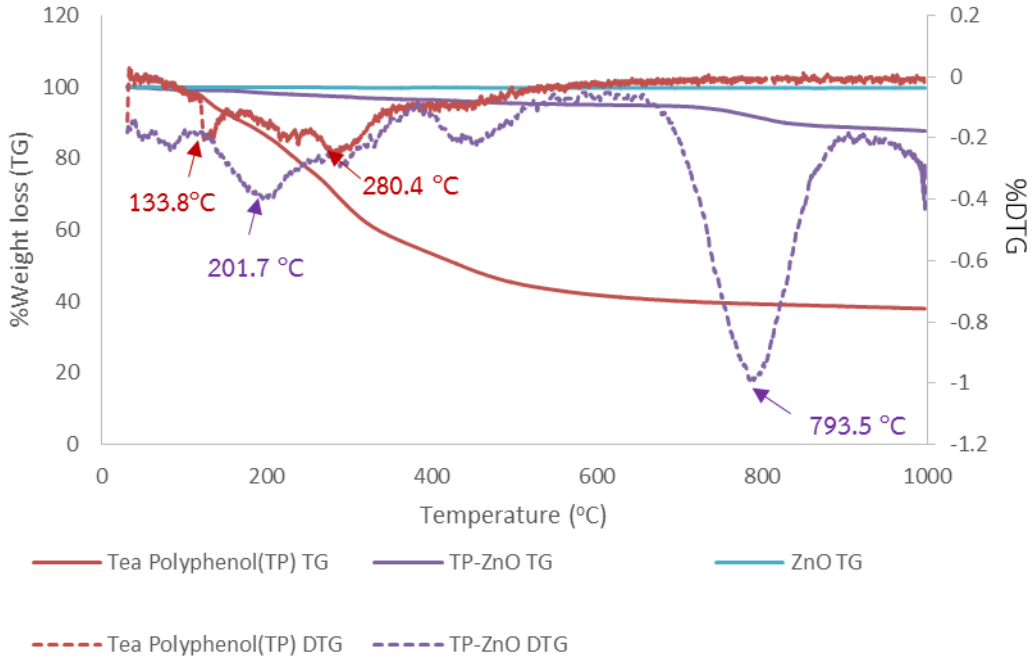

Figure 3.13 Thermo gravimetric curves (TG) and Differential themo gravimetric (DTG) curves of free tea polyphenol (red line), TP-ZnO (purple line) and standard zinc oxide (pale blue line).

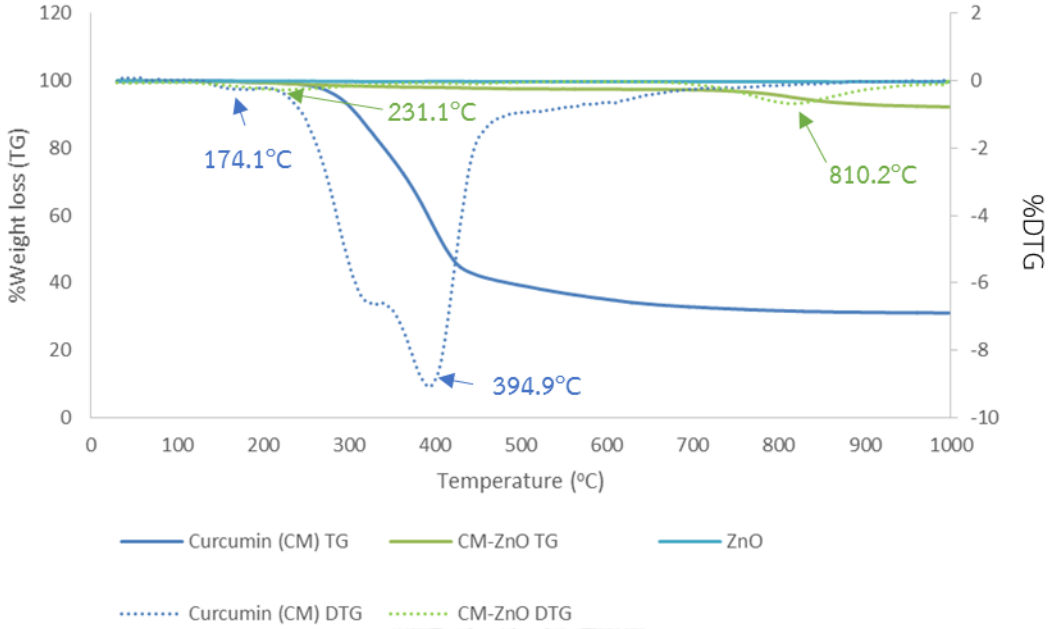

Figure 3.14 Thermo gravimetric curves (TG) and Differential themo gravimetric (DTG) curves of free curcumin (yellow line) and CM-ZnO (red line).

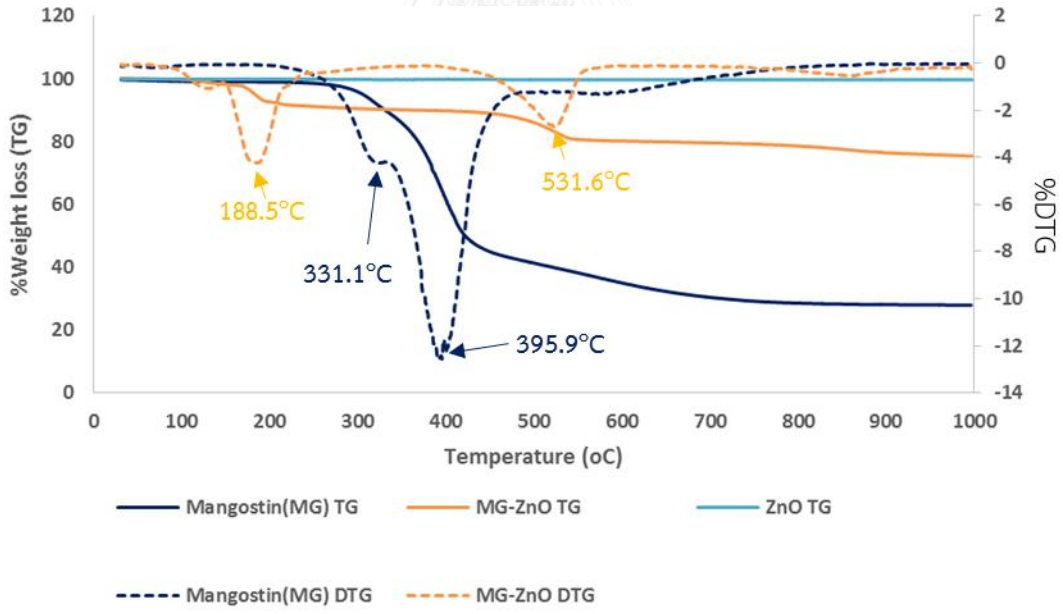

Figure 3.15 Thermo gravimetric curves (TG) and Differential thermo gravimetric (DTG) curves of free α-mangostin (purple line), MG-ZnO (green line) and standard zinc oxide (pale blue line)

The usual characteristic endothermic absorption peak of each natural organic compounds (tea polyphenol at 111.7 °C, curcumin at 178 °C and α-mangostin at 172.9 °C) could not be observed in the particles. Instead, the melting peaks at 160.1°C, and 177.7°C, were observed for TP-ZnO, CM-ZnO, respectively, and 179.6°C and 185.6°C for MG-ZnO nanoparticles. Since, the endothermic peaks of zinc oxide standards were observed at 262.5°C. We speculated that these unknown absorption peaks belonged to the organic matters within the particles after being incorporated within the TP-ZnO, CM-ZnO and MG-ZnO nanoparticles, indicated strong interaction between organic matter and zinc oxide crystals

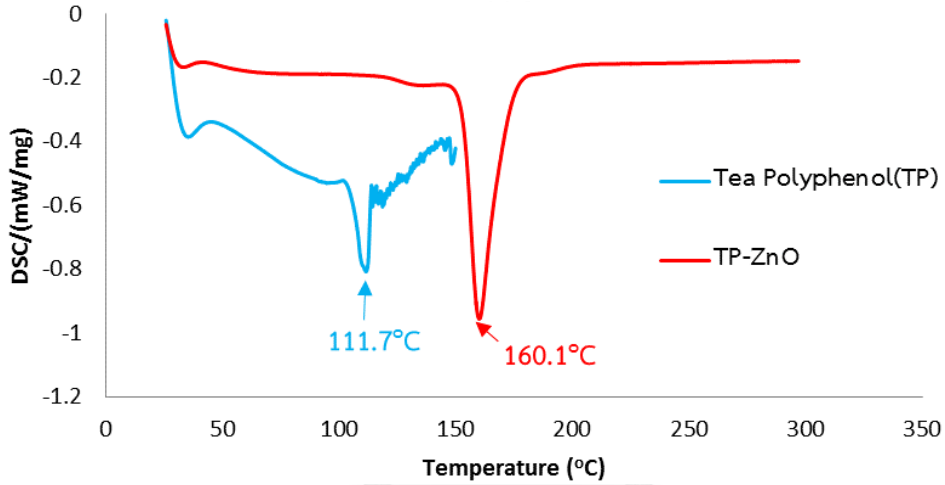

Figure 3.16 Differential scanning calorimetric thermaograms of tea polyphenol(blue line), TP-ZnO (red line) and standard ZnO (green line)

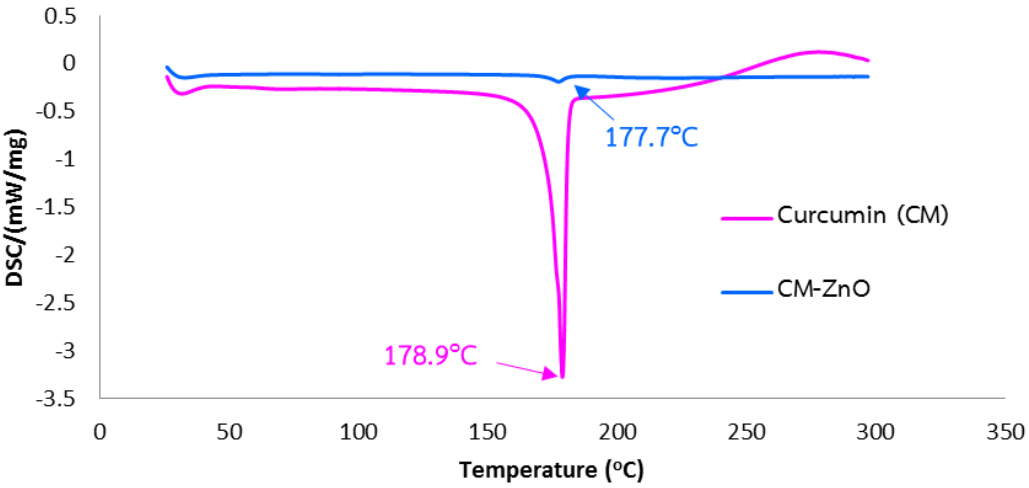

Figure 3.17 Differential scanning calorimetric thermaograms of curcumin(pink line) and CM-ZnO (blue line).

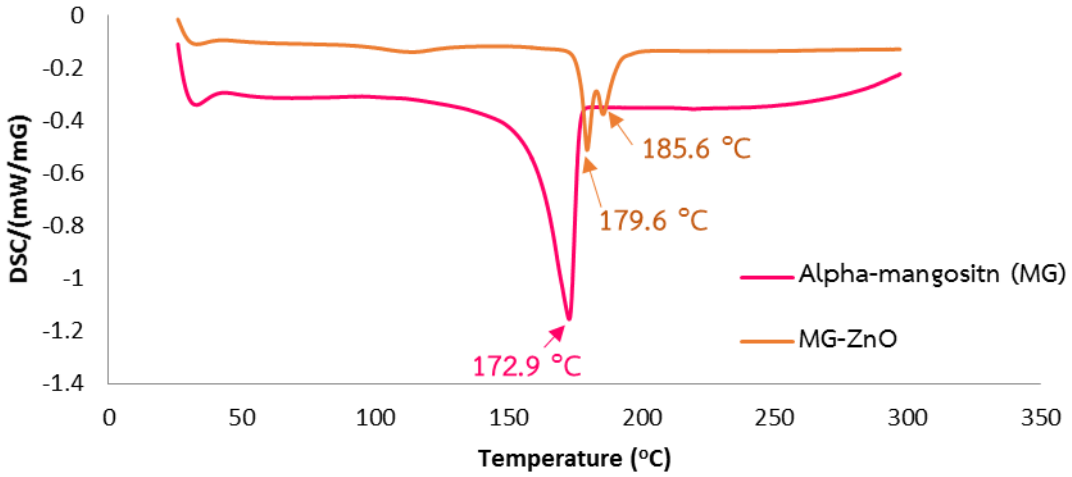

Figure 3.18 Differential scanning calorimetric thermaograms of α-mangostin(pink line) and MG-ZnO (brown line).

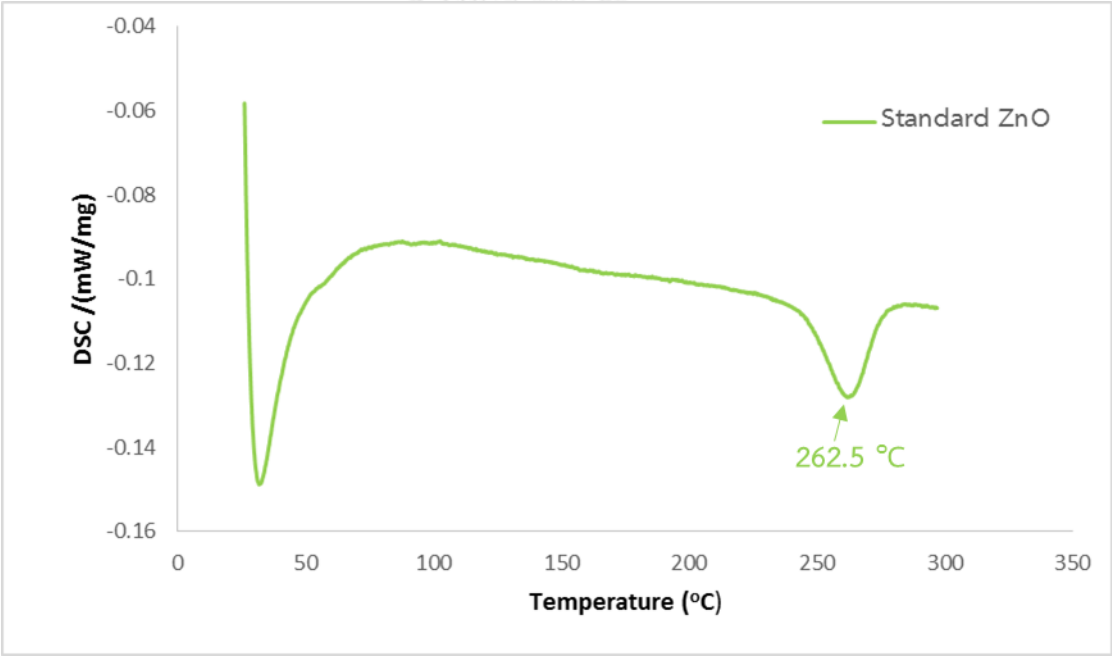

Figure 3.19 Differential scanning calorimetric thermaograms of Standard ZnO (green line)

3.9 Functional group on surface of all particles (TP-ZnO, CM-ZnO and MG-ZnO nanoparticles)

The functional groups on surface of all particles were identified by x-ray photoelectron spectroscopy. The photoelectrons are ejected from different electronic level of each atom. The usual XPS spectrum is a plot of intensity versus binding energy. The binding energy peak indicates where the photoelectron was emitted. Thus, the chemicals bonding of each functional groups exhibited the specific binding energy.

The deconvoluted C1s XPS spectra of TP-ZnO (Figure 3.19, row A) nanoparticles showed the four binding energies peaks at 281.1 eV, 282.3 eV, 283.5 eV and 286.1 eV, corresponding to C-Zn, C-C sp^3, C-C sp^2 and C=C, respectively. The deconvoluted O1s XPS spectrum of TP-ZnO exhibited the binding energy at 527.5eV (O-Zn), 527.9 eV (O=C-O-Zn from carboxyl group) and 529.1 (C-O, OH). The C1S XPS spectra of CM-ZnO (Figure 3.11, row B) showed three peaks at binding energy of 281.9 eV (C-C sp^3), 282.9 eV (C-C sp^2) and 285.3 eV (C-O). Two oxygen species at binding energy peaks in O1s XPS spectra of 526.7 eV (O-Zn) and 528.0 eV (C-O-Zn) were observed for CM-ZnO. The four binding energy peaks of C1s spectra at 281.2 eV (C-Zn), 281.7 eV(C-C sp^3), 283.1 eV (C-C sp^2) and 285.1 eV (C-O) were observed for MG-ZnO (Figure 3.11, row C). The binding energy at 527.3 eV (O-Zn), 528.7 eV(C-O-Zn), 529.1 eV (C-O, OH) and 530.1 eV (C=O) were observed in O1s spectra of the MG-ZnO particles.

จุฬาลงกรณ์มหาวิทยาลัย
CHULALONGKORN UNIVERSITY

As the results, all three particles contained the hydrophillic functional group such as –OH (hydroxyl group) and carbonyl groups at their surfaces. This makes them water dispersible. In addition, the existence of C=C on the surface also allows for the **π-π** interaction. This helps explaining the loading of paclitaxel onto the particles. The hydroxyl functionality also allow for future modification of the materials.

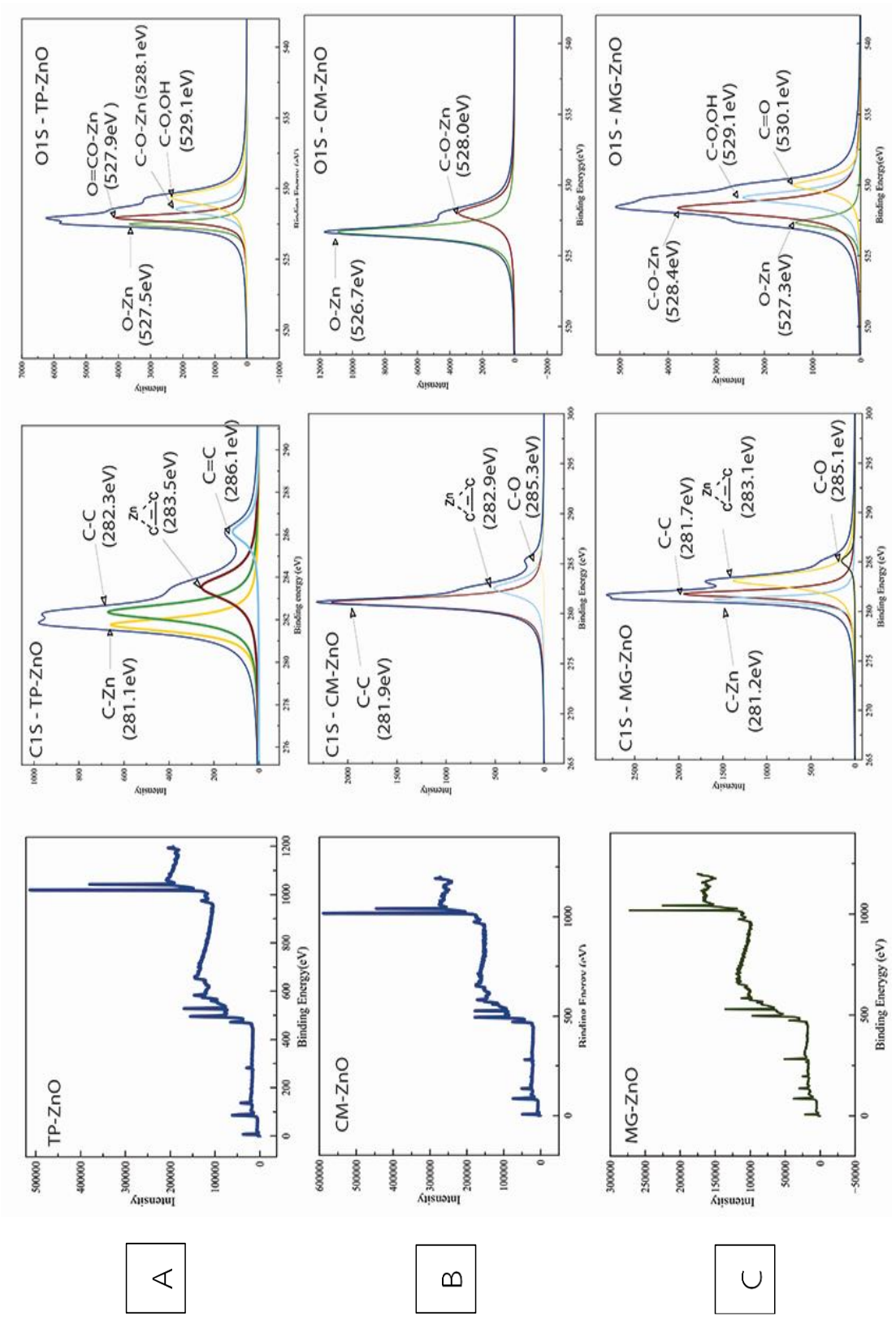

Figure3.20 XPS spectra of TP-ZnO nanoparticles (row A), CM-ZnO nanoparticles (row B) and MG-ZnO nanoparticles (row C).

3.10 Loading of drugs on TP-ZnO nanoparticles

Centrifugation of the mixture of particles allowed separation of the unloaded doxorubicin and paclitaxel from the particles. The percentage of encapsulation efficiency (%EE) of the encapsulation process and loading capacity of the particles were analyzed by quantifying the unloaded doxorubin and paclitaxel by UV-Visible spectroscopy (Table. 3.3). The process of loaded doxorubicin and paclitaxel on the TP-ZnO nanoparticles gave the percentage of encapsulation efficiency at 74.91 ± 1.59 and 71.42 ± 1.74. The loading capability of both loaded nanoparticles exhibited 6.97 ± 0.13 and 6.67 ± 0.15 for loaded doxorubicin and paclitaxel TP-ZnO nanoparticles, respectively.

Table 3.4 Encapsulation efficiency and loading capacity of doxorubicin and paclitaxel on the TP-ZnO nanoparticles.

	%EE		%loading	
	Doxorubicin	Paclitaxel	Doxorubicin	Paclitaxel
TP-ZnO nanoparticles	74.91 ± 1.59	71.42 ± 1.74	6.97 ± 0.13	6.67 ± 0.15

จุฬาลงกรณ์มหาวิทยาลัย
Chulalongkorn University

3.11 Interaction of the cancer drug with TP-ZnO nanoparticles

When doxorubicin and paclitaxel were incubated with TP-ZnO nanoparicles, the drug could be loaded onto the particles at the loading content of 6.97 ± 0.13%w/w with the loading efficiency of 74.91 ± 1.59 %w/w from the loading of doxorubicin and the loading content of paclitaxel at 6.67 ± 0.15 %w/w with the loading efficiency of 71.42 ± 1.74%w/w. These numbers were obtained from the quantitation of unloaded of drug through uv-visible spectroscopic method.

The chemical interaction of the loaded doxorubin on the particles were proofed by FT-IR spectroscopy (Figure 3.20). The interaction of doxorubicin with TP-ZnO particles was evidenced through the disappearance of the C=O stretching peak (1721.21 cm^{-1}) of doxorubicin in the FTIR of product. In addition, shifting of the C=C stretching of the doxorubicin from 1579.61 cm^{-1} in the free drug to 1571.99 cm^{-1} in the complex was also observed (Figure 3.6). We speculated very strong interaction through the carbonyl of doxorubicin with ZnO crystal, probably a very good coordination interaction.

The paclitaxel loaded TP-ZnO nanoparticles also showed good interaction between the loaded drug and the particle through FT-IR spectra (Figure 3.21). The interaction was evidenced through the shifting of C=C stretching from 1645.57 cm^{-1} to 1635.42 cm^{-1}. This indicated that the C=C functionality in paclitaxel, was responsible for the interaction with the particles.

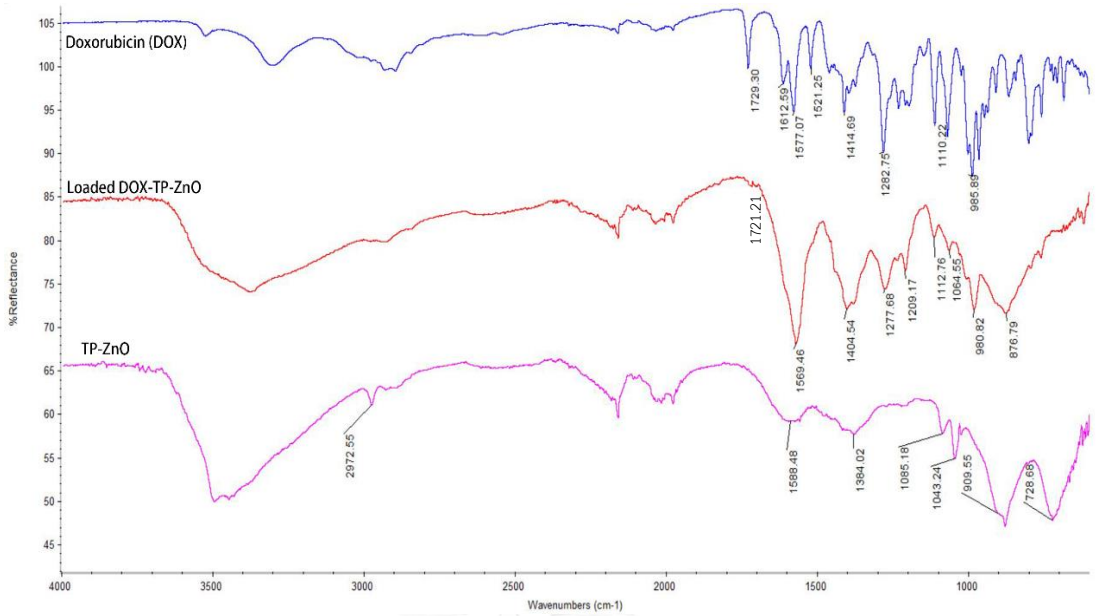

Figure 3.21 FT-IR spectra of doxorubicin (purple line), doxorubicin-loaded TP-ZnO nanoparticles (6.97±0.13 %w/w loading content, red line) and TP-ZnO nanoparticles (pink line).

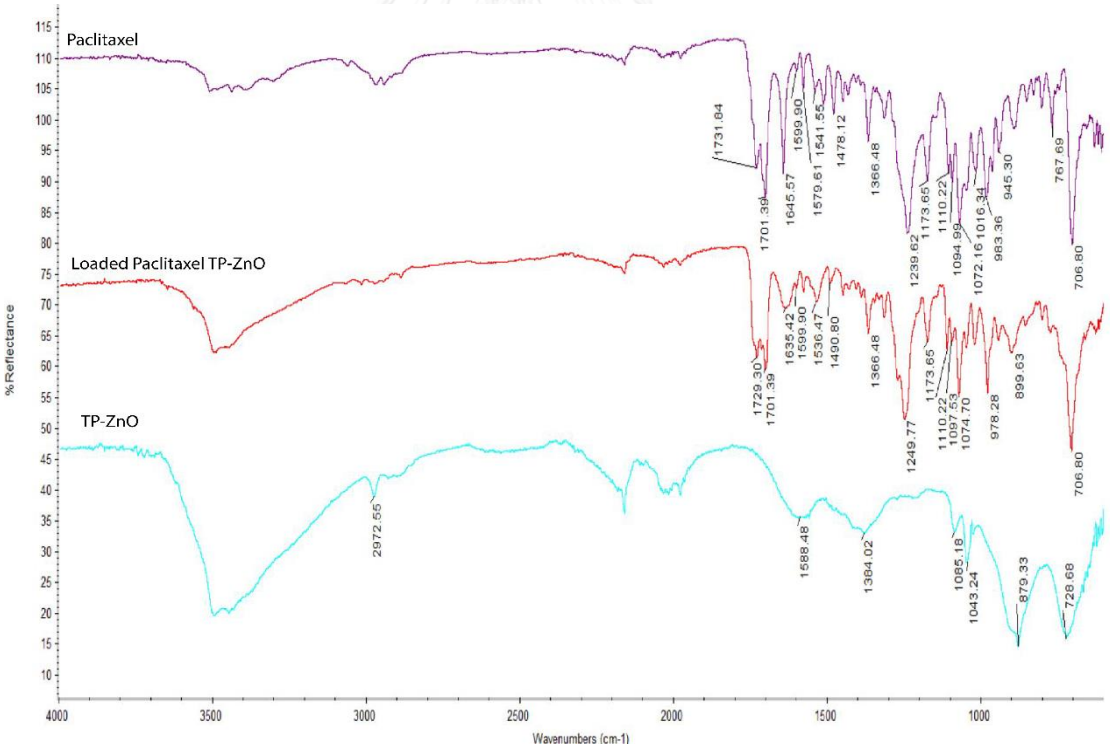

Figure 3.22 FT-IR spectra of paclitaxel (purple line), paclitaxel-loaded TP-ZnO nanoparticles (6.67±0.15%w/w loading content, red line) and unloaded TP-ZnO nanoparticles (blue line).

3.12 pH responsive dissolution test using turbidity measurement

The turbidity of all products was performed by the modified Hach method [31]. The Hach method is EPA-approved turbidity measurement method. The measurement was performed to quantify the transmission of red light (630nm) through the tested sample.

All zinc oxide sample suspensions exhibit strong opaque appearance (pH = 7, Figure 3.22). The opacity of all product suspensions decreased with decreasing pH. Clear solution was observed at pH=4.5 (Figure 3.22). The TP-ZnO (purple line, Figure 3.23), EGCG-ZnO (yellow line, Figure 3.23), CM-ZnO (red line, Figure 3.23) and MG-ZnO (green line) suspensions (pH=7) display low transmission of red light. This indicated pH responsive dissolution of all hybrid ZnO nanoparticles.

The drug-loaded nanoparticles (Figure 3.24-25), the TP-ZnO-DOX as doxorubicin loaded TP-ZnO (gray line, Figure 3.24), and TP-ZnO-TX as the paclitaxel loaded TP-ZnO nanoparticles (red line, Figure 3.25) and the unloaded TP-ZnO particles were compared for their acid responsiveness. It was found that paclitaxel can help delaying the dissolution of the particles during the decrease of the pH. We speculated that the hydrophobic drug loading on the particles can protect the particle from water solvation. Thus the acid disintegration of the hydrophobic drug-loaded particles is delay.

Chulalongkorn University

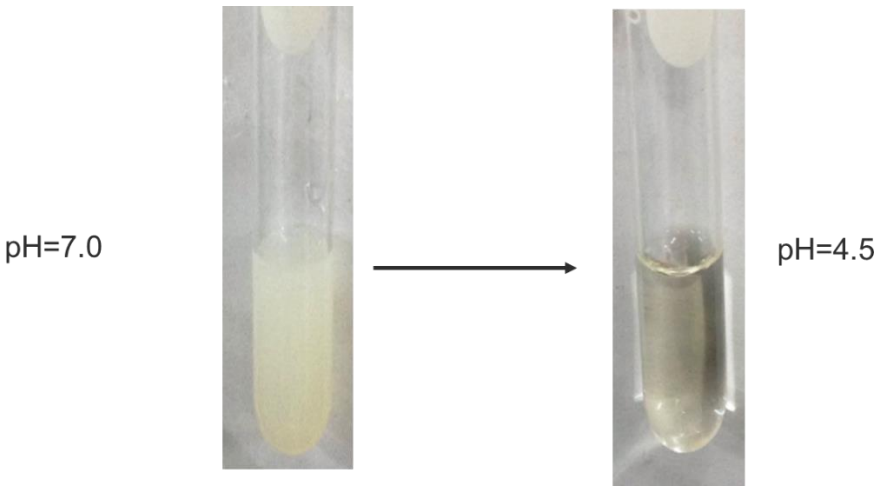

Figure 3.23 Physical appearance of particles at pH=7 (left side) and pH=4.5 (right side).

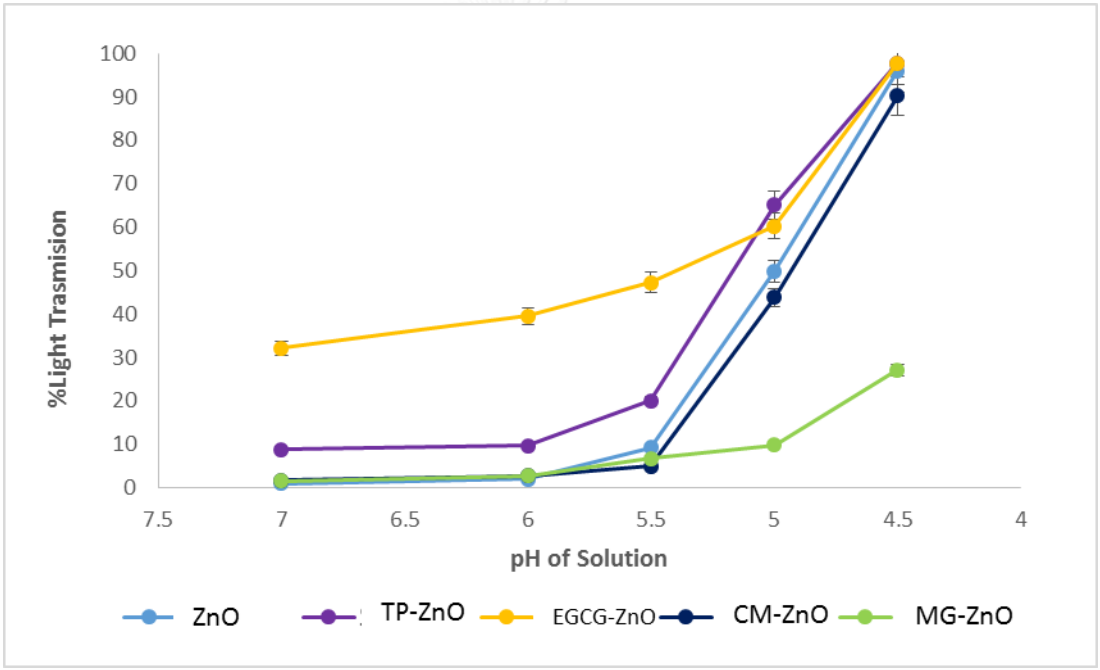

Figure 3.24 Light transmission through ZnO(blue line), TP-ZnO(purple line), EGCG-ZnO(yellow line), CM-ZnO(deep blue line) and MG-ZnO(green line) suspensions.

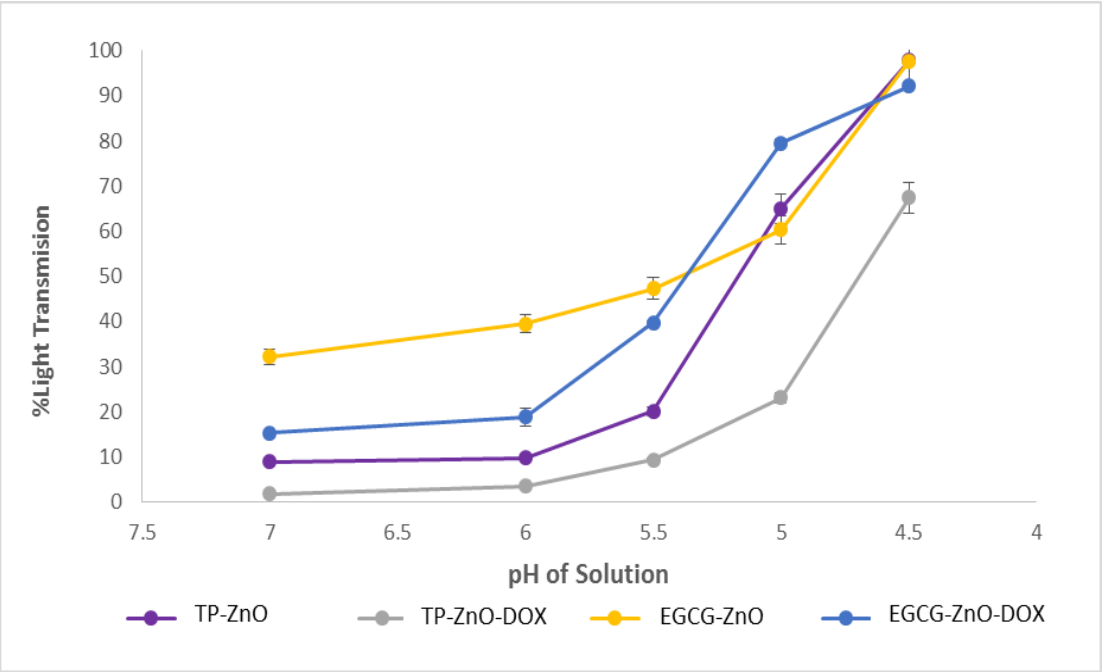

Figure 3.25 Light transmission through EGCG-ZnO(yellow line), TP-ZnO(purple line), TP-ZnO-DOX (gray line) and EGCG-ZnO-DOX(blue line)

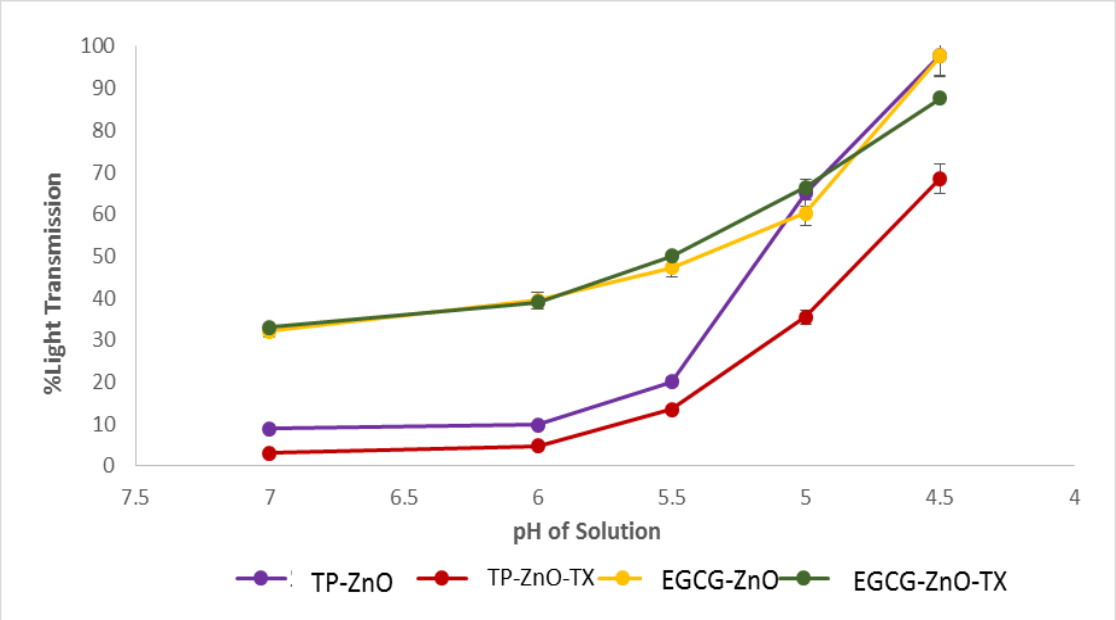

Figure 3.26 Light transmission through EGCG-ZnO(yellow line), TP-ZnO(purple line), TP-ZnO-TX (red line) and EGCG-ZnO-TX(green line)

3.13 Cytotoxicity test with cancer cells

3.13.1 Cytotoxicity test of ZnO, TP-ZnO, EGCG-ZnO nanoparticles, tea polyphenol extract and epigallocatechin-3-gallate free compound.

The ZnO (Figure 3.22, blue column), TP-ZnO(Figure 3.22, purple column), EGCG-ZnO (Figure 3.24, purple column) nanoparticles and free compounds (tea polyphenol extract(TP) and EGCG) were tested on the PC-3 cell at $1x10^4$ cell in 96 well plates. The MTT assay was selected to study the anti-tumor of all products. The MTT assay is designed to quantify cell viability of PC-3 cells. The various concentrations of ZnO, TP-ZnO, EGCG-ZnO (3.1-50 µg/ml) nanoparticles incubated with PC-3 cell with incubation time at 72h.

The ZnO (Figure 3.22, blue column) nanoparticles begin the inhibition of cell viability of PC-3 cell at 12.5 µg/ml at 80% cell viability. The TP-ZnO (Figure 3.22, purple column) nanoparticles could inhibit the PC-3 cells survive at the concentration of TP-ZnO particles at 6.25 µg/ml (concentration of ZnO = 6.19 µg/ml and TP = 0.0606 µg/ml), display the 80% cell viability. The EGCG-ZnO (Figure 3.24, purple column) nanoparticles showed the inhibition cell survive at concentration of particles 12.5 µg/ml (concentration of ZnO =12.39 µg/ml and EGCG = 0.11 µg/ml). When the concentration of particles (ZnO, TP-ZnO and EGCG-ZnO nanoparticles increased, the cytotoxicity of all particles products showed high cytotoxicity because the cell viabilities less than 30%. In contrast, the free forms of EGCG (Figure 3.22, green column, 0.0303-0.485 µg/ml) and tea polyphenol extract (Figure 3.24, green column 0.0275-0.44 µg/ml) at the same concentration in particles showed the low cytotoxicity because cell viability were more than 80%.

3.13.2 Cytotoxicity test of paclitaxel loaded TP-ZnO (TP-ZnO-TX) and doxorubicin TP-ZnO (TP-ZnO-DOX).

The cytotoxicity of drug loaded particles also used MTT assay to study toxicity. The various concentration of drugs loaded particles (3.125-50 μg/ml) were incubated with PC-3 for 72h.

At the same concentration of particles, the both of drugs loaded particles exhibited lower cytotoxicity with PC-3 than unloaded drug particles. Because, we suggested the particles uptake mechanism to cell through the endocytosis pathway. The particles could make endosome burst by the particles dissolve in acidic aqueous solution inside endosome/lysosome. The osmotic pressure inside the endosome increased the endosome could burst to release chemicals out to cytosol. Thus, the results implied that the both of drugs could reduce the endosome burst and showed the low cytotoxicity by the prevention of the particles interact with acidic aqueous solution. Thus, the both of drugs loading could not display the synergistic effect. The investigation of type of drugs for loading on particles still be interested.

As mentioned earlier that the rationale here is that the nanoparticles might be able to get into PC-3 through endocytosis pathway to burst the endosome and to release the substances out. Thus, we verified that the particles could get into the PC-3 cells by endocytosis mechanism.

จุฬาลงกรณ์มหาวิทยาลัย
Chulalongkorn University

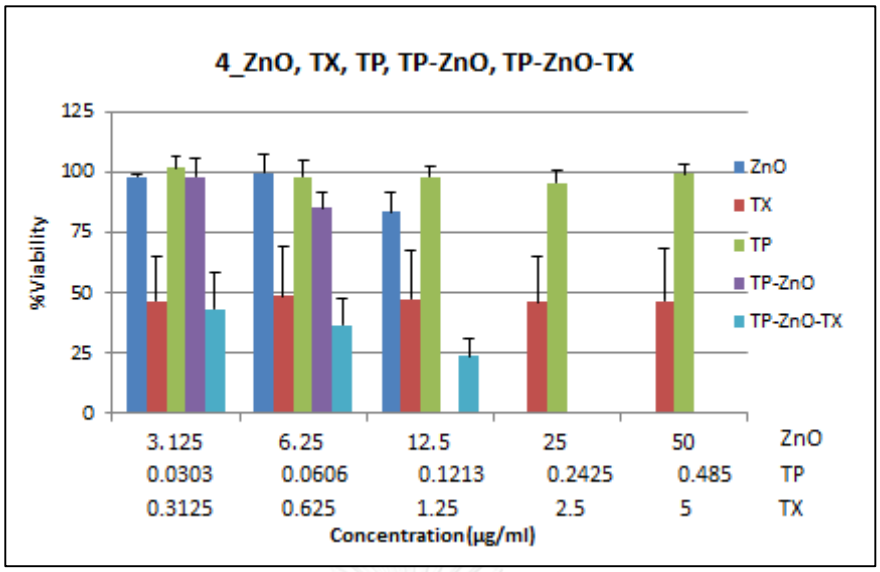

Figure 3.27 Cell viability of PC-3 cancer cell with zinc oxide crystal standard (ZnO, blue column), paclitaxel (TX, red column), tea polyphenol extract (TP, green column), TP-ZnO nanoparticles (purple column) and paclitaxel loaded TP-ZnO (TP-ZnO-TX, light blue column).

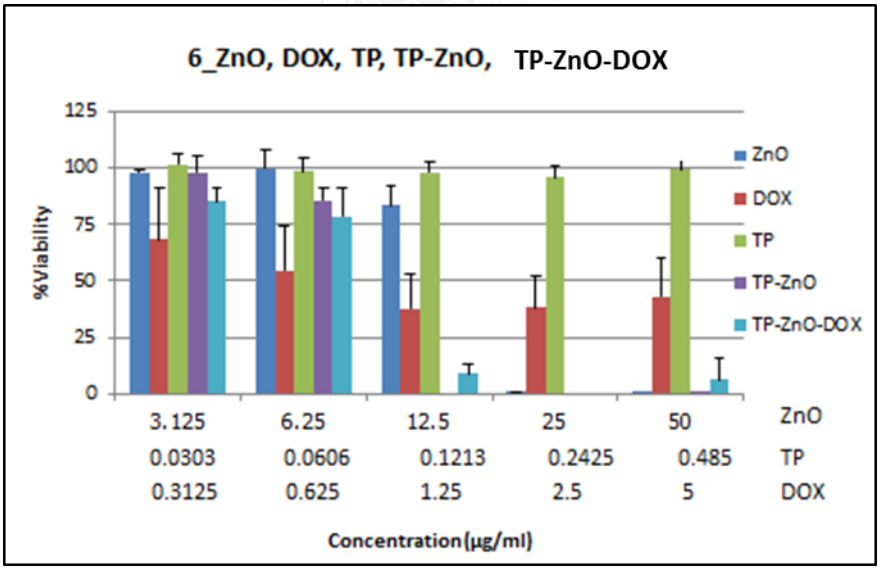

Figure 3.28 Cell viability of PC-3 cancer cell with zinc oxide crystal standard (ZnO, blue column), doxorubicin (DOX, red column), tea polyphenol extract (TP, green column), TP-ZnO nanoparticles (purple column) and doxorubicin loaded TP-ZnO (TP-ZnO-DOX, light blue column).

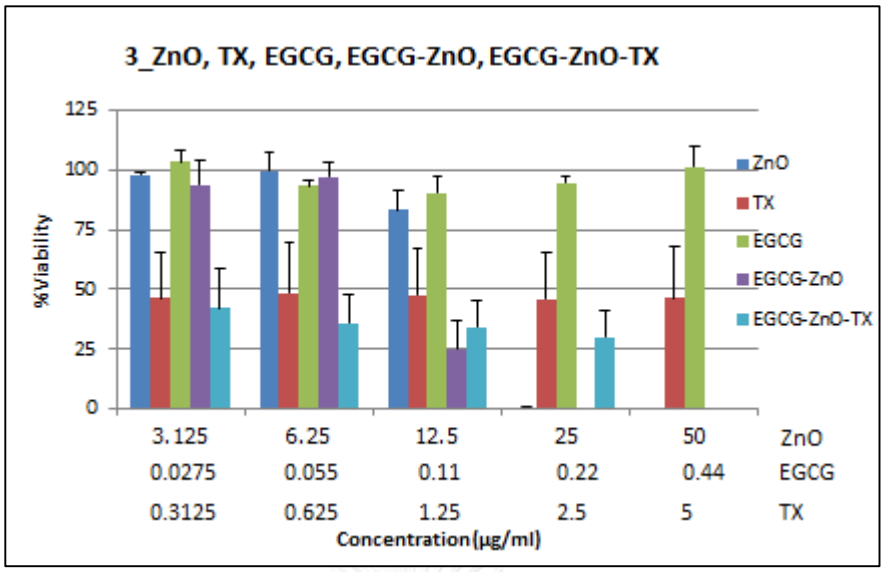

Figure 3.29 Cell viability of PC-3 cancer cell with zinc oxide crystal standard (ZnO, blue column), paclitaxel (TX, red column), epigallocatechin-3-gallate (EGCG, green column), EGCG-ZnO nanoparticles (purple column) and paclitaxel loaded EGCG-ZnO nanoparticles (TP-ZnO-TX, light blue column).

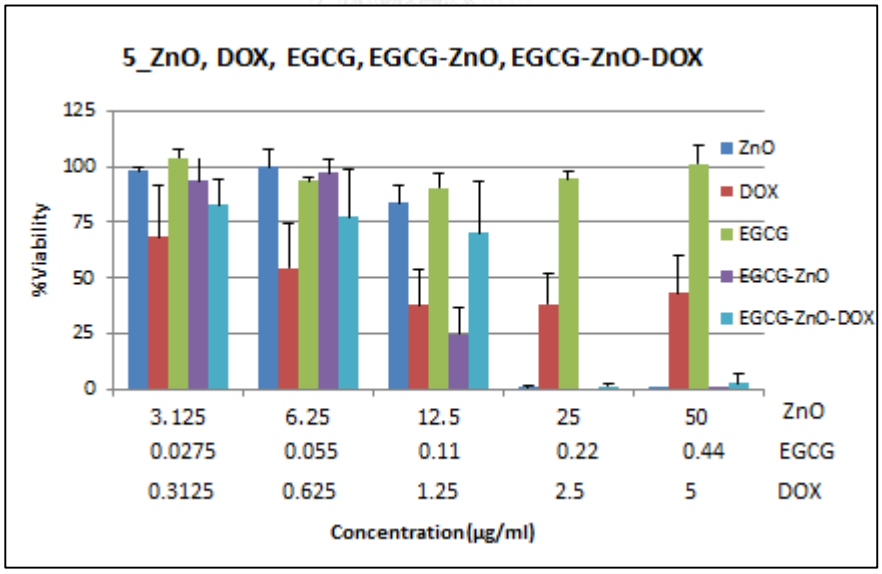

Figure 3.30 Cell viability of PC-3 cancer cell with zinc oxide crystal standard (ZnO, blue column), doxorubicin (DOX, red column), epigallocatechin-3-gallate (EGCG, green column), EGCG-ZnO nanoparticles (purple column) and doxorubicin loaded EGCG-ZnO nanoparticles (EGCG-ZnO-TX, light blue column).

3.14 Cellular uptake of loaded DOX-TP-ZnO

The cellular uptake of DOX-loaded TP-ZnO into PC-3 cell line was monitored using the laser confocal scanning microscopy (CLSM) by detection of the fluorescence of Zn^{2+} probe, zinquin at excitation wavelength of 405 nm and emission wavelength of 450 nm. The doxorubicin as the model drug display the fluorescent image at 570 nm (excitation wavelength at 473 nm). The endosome and lysosome compartments were tracked by early endosome specific dye and lysotracter deep red at excitation 559 nm and 635 nm, and emission at 570 nm for fluorescence from endosome and 658 nm from fluorescence of lysosome. The DOX-loaded TP-ZnO nanoparticles were incubated with PC-3 cells at the cell density of $8x10^4$ cells per well for 8 h at the final of DOX-loaded TP-ZnO concentration of 150 µg/ml (concentration of DOX of 100 ppm and concentration of TP-ZnO of 1000 ppm).

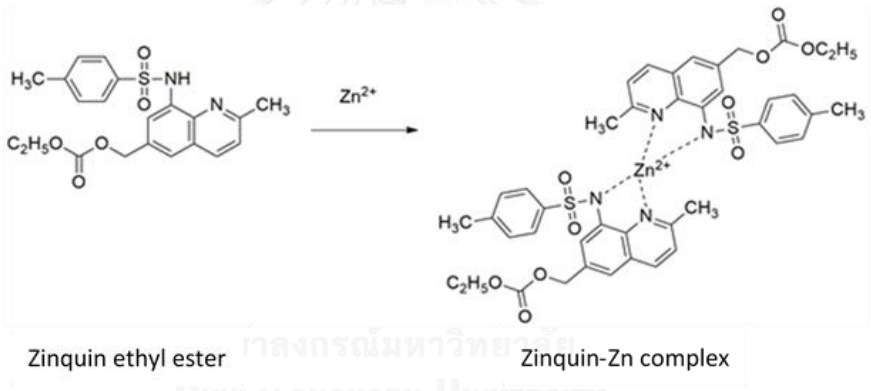

Figure 3.31 The complexation of zinc ions with zinquin ethyl ester

The CLSM images of control PC-3 cells (Figure 3.20) at 0 h (untreated cells) showed no fluorescence signal. When the time elapse, the florescence signal of Zn^{2+} ions gradually increased. Since, this situation appear through the particles solvation in the acid condition in acid compartments (endosome or lysosome). The cellular uptake of DOX-loaded TP-ZnO nanoparticles was clearly observed by fluorescent signals of Zn^{2+} complex with zinquin dye and doxorubicin on the particles. The colocalization of endosome (pH=6.0-5.5), Zn^{2+} ions and doxorubicin fluorescent signals (Figure 3.28, arrow A) display the loaded nanoparticles had ability to enter into cells. As the results, we speculated from the fluorescent evidences that the mechanism of the cellular uptake of this loaded drug nanoparticles as endocytosis pathway. The releasing

mechanism of this particles was explained by the particles response with pH inside the endosome/lysosome compartments.

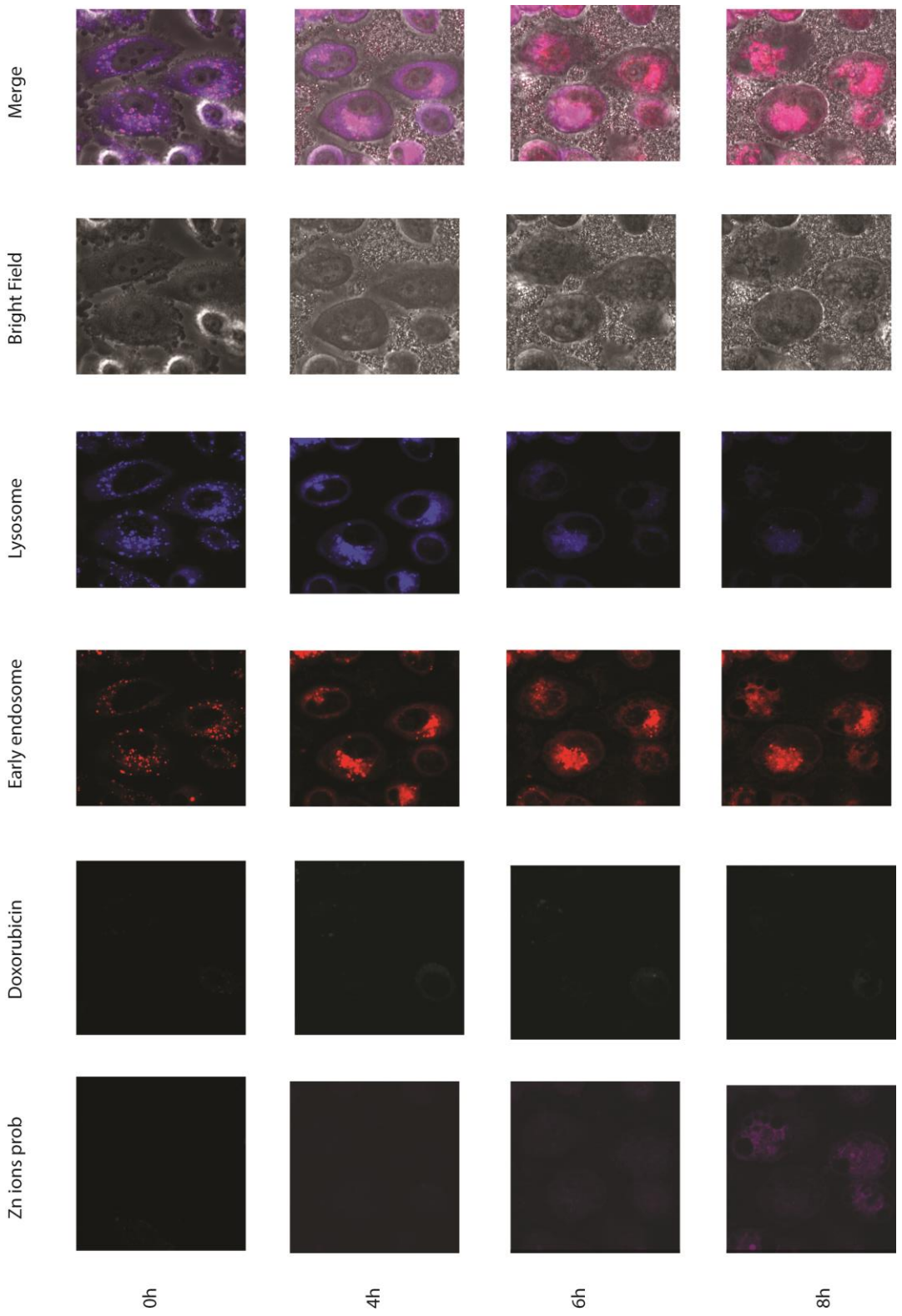

Figure 3.32 The confocal fluorescent picture: Zn^{2+} ions probs (first column), doxorubicin (second column), early endosome (third column), lysosome (fourth column), bright field (fifth column) and merge image (sixth column)

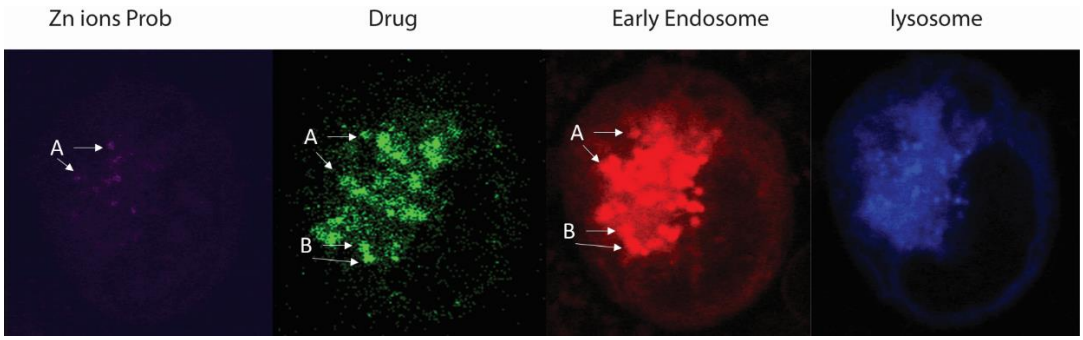

Figure 3.33 The confocal fluorescent focus single cell images: Zn^{2+} ions prob (First column), doxorubicin (second column), early endosome (third column) and lysosome (fouth column).

จุฬาลงกรณ์มหาวิทยาลัย
Chulalongkorn University

CHAPTER IV

CONCLUSION

The result of tea polyphenol extract was extracted from Oonlong tea leaves. The major component in the extract was epigallocatechin-3-gallate at 24.48% w/w. We have successfully fabricated the polyphenol-zinc oxide hybrid nanoparticles. The weight ratio of tea polyphenol extract per zinc chloride at 1:32 and 1:16 exhibited spherical morphology and particles size at 16 and 66 nm, respectively. At high and low concentration of tea polyphenol, the nanostructural product cannot form at spherical architecture. The hybrid curcumin-zinc oxide nanoparticles display the as hexagonal rod architecture (Figure 4.1B).The hybrid α-mangostin-zinc oxide exhibit square prism shape (Figure4.1 A). In addition, the drug loaded TP-ZnO nanoparticles showed that the low cytotoxicity than unloaded drug TP-ZnO nanoparticles. The cellular uptake study of doxorubicin loaded TP-ZnO nanoparticles showed that the particles could be taken up into PC-3 cancer cells through endocytosis mechanism. The particles also display the pH triggered particles that make the endosome burst and release the substance to cytosol. It is possible these particles could apply as anticancer agents. The particles also handle the drug into cell and release to cytosol. We evaluate anti cancer activity only TP-ZnO nanoparticles, not CM-ZnO and MG-ZnO, because, the two later were fabricated from our curiosity and it could induce the zinc oxide nanoparticles formation. We speculate the anti-acne application for MG-ZnO nanoparticles and sun screen application for CM-ZnO nanoparticles. These should be determine in the future.

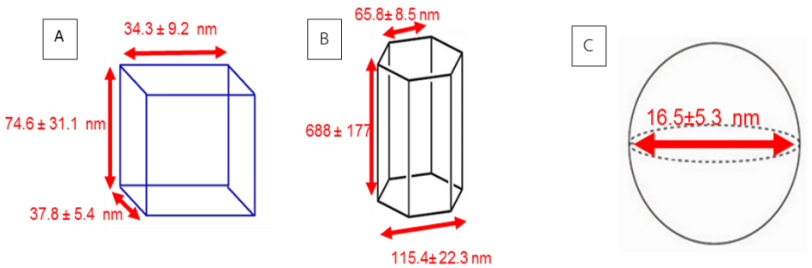

Figure 4.1 The dimension and of each product (A) Mangostin-zinc oxide (MG-ZnO), (B) Curcumin-zinc oxide (CM-ZnO) and (C) Tea polyphenol zinc oxide (TP-ZnO)

APPENDIX

จุฬาลงกรณ์มหาวิทยาลัย
Chulalongkorn University

APPENDIX A

Calculation of %encapsulation efficiency and loading content of drug loaded on the particles

Calibration curve of doxorubicin

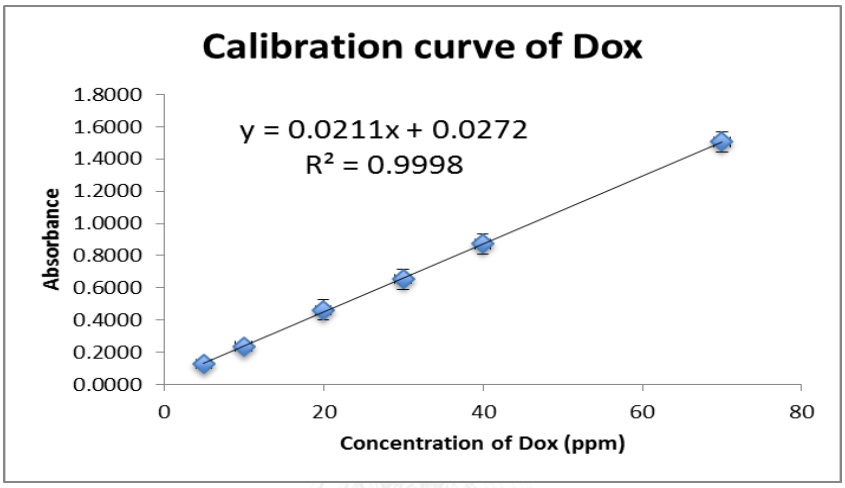

Figure A-1 Calibration curve of doxorubicin at 230.nm

By plotting a graph between absorbance and concentration of doxorubicin solution, a linear relationship was obtained and for calculation of concentration of doxorubicin.

From the equation of calibration curve;

Y=0.0211x+0.0272 (1)

The amount of doxorubicin at the outside of particles was calculated by equation (1)

0.272=0.0211x+0.0272

X=11.60 ppm = 11.60 µg/ml = 0.01160 mg/ml

In final volume of 1000 µl had doxorubicin of (0.01160mg/ml x 1ml) = 0.01160 mg

Weight of loaded doxorubicin = 0.05 – 0.0116 = 0.0384 mg

$$\%Encapsulation\ efficiency = \frac{Weight\ of\ Dox\ found\ in\ paritcles}{Weight\ of\ Initially\ used} \times 100$$

= (0.0384/0.05) x 100

= 76.8%

$$\%Loading = \frac{Weight\ of\ Dox\ found\ in\ paritcles}{Weight\ of\ Dox{-}loaded\ particles} \times 100 \quad (2)$$

= (0.0384/(0.05+0.5)x100

= 6.98%

จุฬาลงกรณ์มหาวิทยาลัย
Chulalongkorn University

Calibration curve of paclitaxel

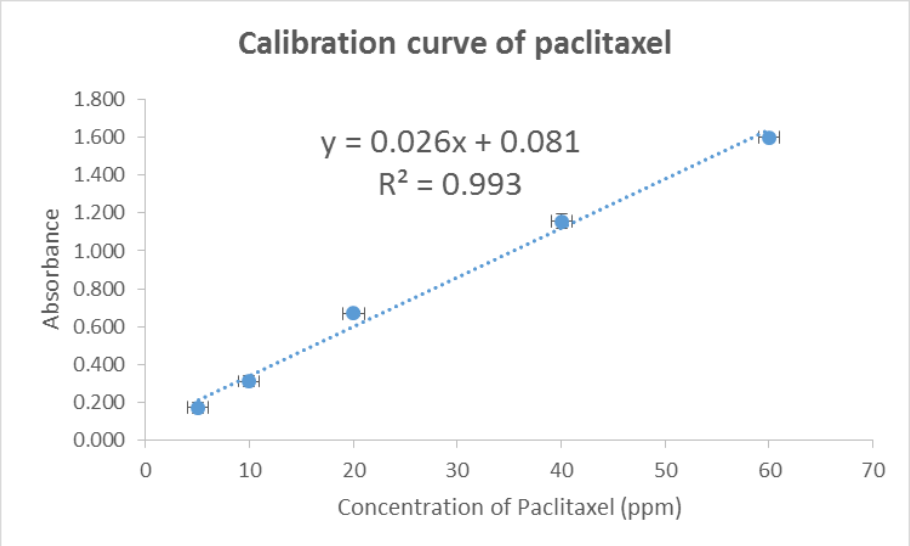

Figure A-2 Calibration curve of paclitaxel at 220.nm

By plotting a graph between absorbance and concentration of paclitaxel solution, a linear relationship was obtained and for calculation of concentration of paclitaxel.

The amount of paclitaxel at the outside of particles was calculated by equation (2)

Y=0.026x + 0.081 (2)

From the equation of calibration curve;

The amount of paclitaxel at the outside of particles was calculated by equation (2)

0.821=0.026x+0.0272

X=30.54 ppm = 30.53 µg/ml = 0.03053mg/ml

In final volume of 1000 µl had paclitaxel of (0.03053mg/ml x 1ml) = 0.03053mg

Weight of loaded doxorubicin = 0.1 – 0.03053 = 0.06947mg

$$\%Encapsulation\ efficiency = \frac{Weight\ of\ paclitaxel\ found\ in\ paritcles}{Weight\ of\ Initially\ used} \times 100$$

= (0.06947/0.1) x 100

= 69.47%

$$\%Loading = \frac{Weight\ of\ paclitaxel\ found\ in\ paritcles}{Weight\ of\ paclitaxel{-}loaded\ particles} \times 100 \quad (2)$$

= (0.06947/(0.1+1)x100

= 6.32%

จุฬาลงกรณ์มหาวิทยาลัย
Chulalongkorn University

APPENDIX B

1. Chemical and culture medium preparation

1.1 Isotonic Phosphate Buffer Saline pH 7.4

NaCl	8.00 g
KCl	0.20 g
KH_2PO_4	0.20 g
Na_2HPO_4	1.44 g

Dissolve NaCl, KCl, KH_2PO_4 and Na_2HPO_4 with distilled water then adjust volume to 1000 ml with distilled water and the pH is measured by pH meter.

1.2. Preparation of MTT solution

Prepare a 12mM stock solution (5 mg/ml (10x)) by 50 mg of MTT reagent was dissolved in 10 ml of PBS. The solution was stirred until completely dissolved and mixed together. The obtained stock solution was sterilized through a 0.5 μm filter and transferred into aliquot tubes. The stock was stored at 4 °C until used.

จุฬาลงกรณ์มหาวิทยาลัย
Chulalongkorn University

REFERENCES

[1] Kickelbick, G. Introduction to Hybrid Materials. in Hybrid Materials, pp. 1-48: Wiley-VCH Verlag GmbH & Co. KGaA, 2007.

[2] Zhao, Y., Trewyn, B.G., Slowing, I.I., and Lin, V.S.Y. Mesoporous Silica Nanoparticle-Based Double Drug Delivery System for Glucose-Responsive Controlled Release of Insulin and Cyclic AMP. Journal of the American Chemical Society 131(24) (2009): 8398-8400.

[3] Zhao, D., Liu, C.-J., Zhuo, R.-X., and Cheng, S.-X. Alginate/CaCO3 Hybrid Nanoparticles for Efficient Codelivery of Antitumor Gene and Drug. Molecular Pharmaceutics 9(10) (2012): 2887-2893.

[4] Chen, M., Zhao, Y., Yang, W., and Yin, M. UV-Irradiation-Induced Templated/In-Situ Formation of Ultrafine Silver/Polymer Hybrid Nanoparticles as Antibacterial. Langmuir 29(51) (2013): 16018-16024.

[5] Duan, H. and Nie, S. Cell-Penetrating Quantum Dots Based on Multivalent and Endosome-Disrupting Surface Coatings. Journal of the American Chemical Society 129(11) (2007): 3333-3338.

[6] Lee, C.-S., Park, W., Park, S.-j., and Na, K. Endolysosomal environment-responsive photodynamic nanocarrier to enhance cytosolic drug delivery via photosensitizer-mediated membrane disruption. Biomaterials 34(36) (2013): 9227-9236.

[7] Sankaranarayanan, J., Mahmoud, E.A., Kim, G., Morachis, J.M., and Almutairi, A. Multiresponse Strategies To Modulate Burst Degradation and Release from Nanoparticles. ACS Nano 4(10) (2010): 5930-5936.

[8] Wang, Y., et al. pH-sensitive pullulan-based nanoparticles for intracellular drug delivery. Polymer Chemistry 5(2) (2014): 423-432.

[9] Marsh, M. and McMahon, H. The structural era of endocytosis. Science 285(5425) (1999): 215-220.

[10] Mukherjee, S., Ghosh, R.N., and Maxfield, F.R. Endocytosis. Physiological reviews 77(3) (1997): 759-803.

[11] Stoorvogel, W., Strous, G.J., Geuze, H.J., Oorschot, V., and Schwartzt, A.L. Late endosomes derive from early endosomes by maturation. Cell 65(3) (1991): 417-427.

[12] Luzio, J.P., Rous, B.A., Bright, N.A., Pryor, P.R., Mullock, B.M., and Piper, R.C. Lysosome-endosome fusion and lysosome biogenesis. Journal of Cell Science 113(9) (2000): 1515-1524.

[13] Moballegh, A., Shahverdi, H., Aghababazadeh, R., and Mirhabibi, A. ZnO nanoparticles obtained by mechanochemical technique and the optical properties. Surface science 601(13) (2007): 2850-2854.

[14] Stanković, A., Veselinović, L., Škapin, S., Marković, S., and Uskoković, D. Controlled mechanochemically assisted synthesis of ZnO nanopowders in the presence of oxalic acid. Journal of materials science 46(11) (2011): 3716-3724.

[15] Kripal, R., Gupta, A.K., Srivastava, R.K., and Mishra, S.K. Photoconductivity and photoluminescence of ZnO nanoparticles synthesized via co-precipitation method. Spectrochimica Acta Part A: Molecular and Biomolecular Spectroscopy 79(5) (2011): 1605-1612.

[16] Lanje, A.S., Sharma, S.J., Ningthoujam, R.S., Ahn, J.-S., and Pode, R.B. Low temperature dielectric studies of zinc oxide (ZnO) nanoparticles prepared by precipitation method. Advanced Powder Technology 24(1) (2013): 331-335.

[17] Oliveira, A.P.A., Hochepied, J.-F., Grillon, F., and Berger, M.-H. Controlled Precipitation of Zinc Oxide Particles at Room Temperature. Chemistry of Materials 15(16) (2003): 3202-3207.

[18] Gao, Y.P., Sisk, C.N., and Hope-Weeks, L.J. A sol–gel route to synthesize monolithic zinc oxide aerogels. Chemistry of Materials 19(24) (2007): 6007-6011.

[19] Kołodziejczak-Radzimska, A. and Jesionowski, T. Zinc Oxide—From Synthesis to Application: A Review. Materials 7(4) (2014): 2833-2881.

[20] Chen, D., Jiao, X., and Cheng, G. Hydrothermal synthesis of zinc oxide powders with different morphologies. Solid State Communications 113(6) (1999): 363-366.

[21] Dem'Yanets, L., Li, L., and Uvarova, T. Zinc oxide: hydrothermal growth of nano-and bulk crystals and their luminescent properties. Journal of materials science 41(5) (2006): 1439-1444.

[22] Yoshida, T. Leaching of zinc oxide in acidic solution. Materials Transactions 44(12) (2003): 2489-2493.

[23] Bian, S.-W., Mudunkotuwa, I.A., Rupasinghe, T., and Grassian, V.H. Aggregation and dissolution of 4 nm ZnO nanoparticles in aqueous environments: influence of pH, ionic strength, size, and adsorption of humic acid. Langmuir 27(10) (2011): 6059-6068.

[24] Barick, K., Nigam, S., and Bahadur, D. Nanoscale assembly of mesoporous ZnO: a potential drug carrier. Journal of Materials Chemistry 20(31) (2010): 6446-6452.

[25] Muhammad, F., et al. Acid degradable ZnO quantum dots as a platform for targeted delivery of an anticancer drug. Journal of Materials Chemistry 21(35) (2011): 13406-13412.

[26] Zhang, Z.Y., et al. Biodegradable ZnO@ polymer Core–Shell Nanocarriers: pH-Triggered Release of Doxorubicin In Vitro. Angewandte Chemie International Edition 52(15) (2013): 4127-4131.

[27] Uzzo, R.G., et al. Zinc inhibits nuclear factor-**K**B activation and sensitizes prostate cancer cells to cytotoxic agents. Clinical cancer research 8(11) (2002): 3579-3583.

[28] Yang, N., Zhao, B., Rasul, A., Qin, H., Li, J., and Li, X. PIAS1-modulated Smad2/4 complex activation is involved in zinc-induced cancer cell apoptosis. Cell death & disease 4(9) (2013): e811.

[29] Sun, S.l., et al. Free Zn2+ enhances inhibitory effects of EGCG on the growth of PC-3 cells. Molecular nutrition & food research 52(4) (2008): 465-471.

[30] Yang, J., et al. Mechanism of free Zn (2+) enhancing inhibitory effects of EGCG on the growth of PC-3 cells: interactions with mitochondria. Biological trace element research 131(3) (2009): 298-310.

[31] Van Rijn, L.C., van Rijn, L.C., and van Rijn, L.C. Principles of sediment transport in rivers, estuaries and coastal seas. Vol. 1006: Aqua publications Amsterdam, 1993.

VITA

Mister Pawatsanai Samutprasert was born on January 1, 1991 in Bangkok, Thailand. He got a Bachelor's Degree of Science in Chemistry from Chulalongkorn University in 2012. After that, he started his graduate study on a Master's degree in Organic chemistry at Chulalongkorn University. During that time she presented his work in oral presentation in the title of "Zinc oxide-polyphenol nanoparticles and application in drug delivery" in The 5th Asian Symposium on Advanced Materials: Chemistry, Physics & Biomedicine of Functional and Novel Materials (ASAM-5). The financed for joining the conference was supported by the Center of Excellence on Petrochemicals and Materials Technology (Petromat), Chulalongkorn University.

My address is 94/9 Sailuat road, Soi 1, Paknam, Muaeng Samutprakan, Samutprakan, Thailand, 10270

จุฬาลงกรณ์มหาวิทยาลัย
Chulalongkorn University